Developmental Cell

Ankrd11 is a chromatin regulator involved in autism that is essential for neural development

--Manuscript Draft--

Manuscript Number:	DEVELOPMENTAL-CELL-D-14-00584R3
Full Title:	Ankrd11 is a chromatin regulator involved in autism that is essential for neural development
Article Type:	Research Article
Keywords:	Ankrd11; autism spectrum disorder; neurogenesis; cortical development; histone acetylation; Chromatin; HDAC; Neural Stem Cell
Corresponding Author:	Freda Miller Hospital for Sick Children, University of Toronto Toronto, Ontario CANADA
First Author:	Denis Gallagher
Order of Authors:	Denis Gallagher
	Anastassia Voronova
	Mark Andrew Zander
	Gonzalo Ignacio Cancino
	Alexa Bramall
	Matthew Krause
	Clemer Abad
	Mustafa Tekin
	Paul Neilsen
	David C allen
	Stephen Scherer
	Gordon Keller
	David Kaplan
	Katherina Walz
	Freda Miller
Abstract:	Ankrd11 is a potential chromatin regulator implicated in neural development and autism spectrum disorder (ASD) with no known function in the brain. Here, we show that knockdown of Ankrd11 in developing murine or human cortical neural precursors caused decreased proliferation, reduced neurogenesis, and aberrant neuronal positioning. Similar cellular phenotypes and aberrant ASD-like behaviors were observed in Yoda mice carrying a point mutation in the Ankrd11 HDAC-binding domain. Consistent with a role for Ankrd11 in histone acetylation, Ankrd11 was associated with chromatin, colocalized with HDAC3, and expression and histone acetylation of Ankrd11 target genes were altered in Yoda neural precursors. Moreover, the Ankrd11 knockdown-mediated decrease in precursor proliferation was rescued by inhibiting histone acetyltransferase activity or expressing HDAC3. Thus, Ankrd11 is a crucial chromatin regulator that controls histone acetylation and gene expression during neural development, thereby providing a likely explanation for its association with cognitive dysfunction and ASD.

Dear Dan:

Please find attached our revised version of "Ankrd11 is a chromatin regulator involved in autism that is essential for neural development" by Gallagher et al. We would like to thank you for your ongoing help with this manuscript, since by addressing your suggestions we have clarified a number of issues in the manuscript. In particular, we have made two changes in response to your recent letter. First, we replaced the term "epigenetic regulator" with "chromatin regulator" throughout the manuscript. We agree that this is formally more correct. Second, as we discussed, we immunostained appropriately-aged sections of wildtype and Yoda cortices with markers for radial precursors (Pax6), intermediate progenitors (Tbr2) and newborn neurons (Satb2) and used these to define the various cortical regions for the BrdU-labelled sections. We have added this immunostaining as Figures 4F and S3C. We then recounted our sections using these borders. Results of this analysis, shown in Fig. 4H, were very similar to the analysis we had submitted in our last revision, with significantly increased BrdU-positive cells in the IZ, and fewer in the CP. However, while the ultimate results were the same, we feel that the addition of these immunostained sections provides higher confidence in the quantitative data.

We have also ensured that the manuscript and figures meet the formatting requirements as per Developmental Cell guidelines. We hope that the manuscript is now suitable for publication in Developmental Cell, and would again like to thank you for your ongoing help. We believe that the review and editorial process has resulted in a significantly better manuscript.

With kind regards,
Freda

Dear Dan:

Please find attached our revised version of "Ankrd11 is a chromatin regulator involved in autism that is essential for neural development" by Gallagher et al. We would like to thank you for your ongoing help with this manuscript, since by addressing your suggestions we have clarified a number of issues in the manuscript. In particular, we have made two changes in response to your recent letter. First, we replaced the term "epigenetic regulator" with "chromatin regulator" throughout the manuscript. We agree that this is formally more correct. Second, as we discussed, we immunostained appropriately-aged sections of wildtype and Yoda cortices with markers for radial precursors (Pax6), intermediate progenitors (Tbr2) and newborn neurons (Satb2) and used these to define the various cortical regions for the BrdU-labelled sections. We have added this immunostaining as Figures 4F and S3C. We then recounted our sections using these borders. Results of this analysis, shown in Fig. 4H, were very similar to the analysis we had submitted in our last revision, with significantly increased BrdU-positive cells in the IZ, and fewer in the CP. However, while the ultimate results were the same, we feel that the addition of these immunostained sections provides higher confidence in the quantitative data.

We have also ensured that the manuscript and figures meet the formatting requirements as per Developmental Cell guidelines. We hope that the manuscript is now suitable for publication in Developmental Cell, and would again like to thank you for your ongoing help. We believe that the review and editorial process has resulted in a significantly better manuscript.

With kind regards,
Freda

Ankrd11 is a chromatin regulator involved in autism that is essential for neural development

Denis Gallagher[1,3,10], Anastassia Voronova[1,10], Mark A. Zander[1], Gonzalo I. Cancino[1], Alexa Bramall[1], Matthew P. Krause[1], Clemer Abad[4], Mustafa Tekin[4], Paul M. Neilsen[5], David F. Callen[6], Stephen W. Scherer[2,7], Gordon M. Keller[,3,8], David R. Kaplan[1,7] Katherina Walz[4] and Freda D. Miller[1,3,7,9]

Programs in Neuroscience and Mental Health[1] and Genetics and Genome Biology[2], Hospital for Sick Children, Toronto, Canada M5G 1L7, McEwen Center for Regenerative Medicine[3], University Health Network, Toronto, Canada M5G 1L7, Dr. John T. Macdonald Foundation Department of Human Genetics, and John P. Hussman Institute for Human Genomics, Miller School of Medicine, University of Miami, Fl 33136 USA[4], Swinburne University of Technology, Sarawak Campus, Kuching 93350 Sarawak, Malaysia[5], Centre for Personalised Cancer Medicine, University of Adelaide, Adelaide SA 5000[6], Departments of Molecular Genetics[7] , Medical Biophysics[8], and Physiology[9], University of Toronto, Toronto, Canada M5G 1X5.

Co-first author [10]

Correspondence to: Freda D. Miller (Email: **fredam@sickkids.ca**) or David R. Kaplan (Email: **dkaplan@sickkids.ca**)

Running Title: Ankrd11 is a developmental chromatin regulator

SUMMARY

Ankrd11 is a potential chromatin regulator implicated in neural development and autism spectrum disorder (ASD) with no known function in the brain. Here, we show that knockdown of Ankrd11 in developing murine or human cortical neural precursors caused decreased proliferation, reduced neurogenesis, and aberrant neuronal positioning. Similar cellular phenotypes and aberrant ASD-like behaviors were observed in Yoda mice carrying a point mutation in the Ankrd11 HDAC-binding domain. Consistent with a role for Ankrd11 in histone acetylation, Ankrd11 was associated with chromatin, colocalized with HDAC3, and expression and histone acetylation of Ankrd11 target genes were altered in Yoda neural precursors. Moreover, the Ankrd11 knockdown-mediated decrease in precursor proliferation was rescued by inhibiting histone acetyltransferase activity or expressing HDAC3. Thus, Ankrd11 is a crucial chromatin regulator that controls histone acetylation and gene expression during neural development, thereby providing a likely explanation for its association with cognitive dysfunction and ASD.

INTRODUCTION

We currently understand little about mechanisms that are dysregulated in human neurodevelopmental disorders like ASD. In ASD, many different genes are affected by sporadic or rare-inherited DNA sequence mutations or copy number variations (Devlin and Scherer, 2012). Many of these are involved in synapse function, but others, such as Ankyrin repeat domain conaining protein 11 (Ankrd11; Zhang et al., 2004) are associated with transcription or chromatin regulation, but have no known role in the brain (Pinto et al., 2014; Iossifov et al., 2014). In humans, deletion or mutation of one allele of the *ANKRD11* gene causes cognitive dysfunction and ASD (Marshall et al., 2008; Sirmaci et al., 2011; Lo-Castro et al., 2013), and some individuals display corpus callosum hypoplasia and periventricular heterotopias (Willemsen et al., 2010). Intriguingly, cell line studies indicate that Ankrd11 is a large nuclear protein that regulates transcription, potentially by binding chromatin modifying enzymes like histone deacetylases (HDACs) (Zhang et al., 2004, 2007a, 2007b; Li et al., 2008; Neilsen et al. 2008).

Modification of chromatin structure by histone acetylation is essential for nervous system development and function, and plays a particularly important role in neural precursors (Lilja et al., 2013; Rudenko and Tsai 2014; Castelo-Branco et al., 2014). For example, haploinsufficiency for CBP causes cognitive dysfunction in part because it regulates neural precursor development via its histone acetyltransferase (HAT) activity (Wang et al., 2009). HDAC inhibitors and neural-specific knockouts of HDACs 1 and 2 also perturb neural precursor proliferation and differentiation (Lilja et al., 2013), and NCoR, a nuclear coregulator that binds HDACs, is essential for appropriate neural precursor differentiation (Castelo-Branco et al., 2014).

Here, we show that Ankrd11 functions as a nuclear coregulator in the developing brain, regulating histone acetylation and gene expression, and in so doing determining precursor proliferation, neurogenesis, and neuronal positioning. Moreover, we show that when Ankrd11 is decreased or mutated in mice, this perturbs neural development and when mutated, causes aberrant behavior. These findings therefore provide an explanation for the cognitive dysfunction observed when the *ANKRD11* gene is mutated or deleted in humans.

RESULTS

Ankrd11 is expressed in precursors and neurons of the developing murine cortex

To ask about Ankrd11 during neural development, we studied the embryonic cerebral cortex. qPCR and western blots (Figures 1A and 1B) showed expression of Ankrd11 in the embryonic day 11 (E11) through postnatal day 3 (P3) cortex. Immunostaining showed that Ankrd11 was detectable in nuclear foci of precursors in the E12 ventricular and subventricular (VZ/SVZ) zones (Figure 1C). By E16, Ankrd11 was detectable in nuclei of Pax6-positive radial precursors, the stem cells in this system, and βIII-tubulin positive neurons in the cortical plate (Figures 1D and 1E).

Ankrd11 regulates proliferation and neurogenesis in cultured murine cortical precursor cells

To identify a potential function for Ankrd11, we generated two Ankrd11 shRNAs and transfected them into murine NIH/3T3 cells that express endogenous Ankrd11. Western blots showed that both shRNAs were efficacious, and validated the specificity of the Ankrd11 antibody (Figure 1F). We used these shRNAs to ask about Ankrd11's function in E12.5 radial precursors that generate neurons in culture (Barnabé-Heider et al., 2005). Ankrd11 immunoreactivity was readily detectable in nuclei of radial precursors expressing Pax6 and Ki67, and in newborn βIII-tubulin-positive neurons (Figure 1G). When cultures were cotransfected with EGFP and *Ankrd11* shRNAs, the shRNAs significantly decreased the percentage of transfected cells expressing Ankrd11 (Figures 1H and 1I). Ankrd11 knockdown did not affect cell survival, as assessed by counting EGFP-positive cells with condensed, apoptotic nuclei ($p > 0.05$), or by immunostaining for cleaved caspase-3 (Figure S1) 2 days post-transfection. Autophagy was also unchanged, as monitored by LC3 immunoreactivity ($p > 0.05$; data not shown).

Ankrd11 knockdown did affect precursor proliferation, as measured by Ki67 immunoreactivity 2 days post-transfection or by adding BrdU to cultures one day post-transfection and immunostaining for BrdU 2 days later (Figures 1J-L). This was not due to a decrease in Pax6-positive radial precursors, but was caused by a decrease in the radial precursor proliferation index (Figures 1M-O). *Ankrd11* knockdown also reduced transfected βIII-tubulin-positive neurons 3 days post-transfection (Figures 1M and 1P).

Ankrd11 knockdown also decreased radial precursor self-renewal, as shown by clonal

analysis with the *piggybac* (PB) transposon which indelibly marks precursors and their progeny (Gallagher et al., 2013). Specifically, precursors were transfected at low efficiency (Figure S2A) with the PB transposase and PB EGFP reporter, plus control or *Ankrd11* shRNAs, and cultures were immunostained 3 days later for EGFP, the precursor marker Sox2 and βIII-tubulin (Figure 2A). *Ankrd11* knockdown reduced EGFP-positive multicellular clones and the proportion of clones containing a Sox2-positive precursor, while neuron-only clones were increased (Figures 2B-D). The number of precursors in clones containing at least one Sox2-positive cell was also reduced (Figure 2E).

Ankrd11 regulates proliferation and differentiation of human forebrain precursors

Since *ANKRD11* mutations are associated with human ASD, we asked whether Ankrd11 was also required for human embryonic stem (ES) cell-derived cortical precursors, generated as we previously described (Wang et al., 2012). Nuclear Ankrd11 immunoreactivity was detectable in almost all cells in these cultures, including Ki67-positive precursors and βIII-tubulin-positive neurons (Figure 2F). To ask about its function, we generated a human-targeted *Ankrd11* shRNA, and confirmed its efficacy by transfecting it into HEK293 cells that express endogenous Ankrd11 (Figure 2G). We cotransfected this shRNA into human neural precursors together with nuclear EGFP. Immunostaining 3 days later showed that the Ankrd11 shRNA significantly reduced Ankrd11 expression in transfected cells (Figure 2H and S2B), and that this knockdown decreased EGFP-positive, Ki67-positive proliferating precursors and EGFP-positive, βIII-tubulin-positive newborn neurons (Figures 2I-K), as seen in murine precursors.

Ankrd11 knockdown in vivo decreases radial precursor proliferation and neurogenesis and causes mislocalization of cortical neurons

To ask whether Ankrd11 regulates cortical development *in vivo* we *in utero* electroporated E13/14 cortices with nuclear EGFP and control or *Ankrd11* shRNAs and immunostained sections 3 days later. This approach targets radial precursors in the VZ, many of which differentiate into neurons that migrate through the intermediate zone (IZ) to the cortical plate (CP). *Ankrd11* knockdown altered cell location, with more EGFP-positive cells in the VZ/SVZ and fewer in the CP (Figures 2L and 2M). *Ankrd11* knockdown did not alter EGFP-positive, Pax6-positive radial precursor numbers, but it did reduce Ki67-positive proliferating

cells and the radial precursor proliferation index (Figures 2N-Q and S2C). Mitotic cells expressing phospho-histone H3 were also decreased (Figures 2R and S2D).

We immunostained similar sections for the pan-neuronal marker HuD (Figure 3A). *Ankrd11* knockdown decreased EGFP-positive, HuD-positive neurons by almost two-fold, and these neurons were misplaced, with fewer in the CP and more in the VZ/SVZ (Figures 3B and 3C). To define the phenotype of these misplaced neurons, we analyzed the layer-specific markers Satb2 and Tbr1 4 days post-electroporation (Figures 3D and 3E). In controls, Satb2-positive and Tbr1-positive cells comprised about 34% and 8% of EGFP-positive cells (Figure 3F), as expected (Tsui et al., 2013). Following *Ankd11* knockdown, Satb2-positive but not Tbr1-positive neurons were reduced (Figure 3F). However, Tbr1-positive but not Satb2-positive neurons were inappropriately positioned at this timepoint (Figures 3G and S3).

To ask if these neuronal perturbations persisted, we electroporated E13/14 cortices with the PB transposase and PB EGFP reporter, plus control or *Ankrd11* shRNA, and analyzed sections at P3. In controls, almost all EGFP-positive cells were in layers I to III, but following *Ankrd11* knockdown, they were scattered throughout the cortex, including the SVZ (Figures 3H and 3K). As seen earlier, *Ankrd11* knockdown decreased Satb2-positive but not Tbr1-positive neurons, but at this stage both types of cortical neurons were mislocalized to deeper cortical layers and the SVZ (Figures 3I-N).

Yoda mice heterozygous for an Ankrd11 missense mutation in the repressive HDAC binding domain also show decreased precursor proliferation and mislocalized neurons

The Yoda mutant mouse was isolated in an ENU screen for perturbations in bone metabolism (Barbaric et al., 2008), and carries a missense point mutation in the highly-conserved C-terminal repression domain of the *Ankrd11* gene (Figure 4A). Homozygous Yoda mice are embryonic lethal, but heterozygous mice ($Ankrd11^{Yod/+}$) survive into adulthood with altered bone metabolism and craniofacial abnormalities (Barbaric et al., 2008). Intriguingly, a two amino acid deletion in the analogous region has been found in the human gene (Figure 4A) (Sirmaci et al., 2011). To ask if Yoda mice displayed perturbed neural development, we immunostained E18.5 $Ankrd11^{Yod/+}$ cortical sections for Tbr1 and Satb2 (Figures 4B,C). Neurons of both phenotypes were misplaced in the VZ/SVZ of $Ankrd11^{Yod/+}$ cortices (Figures 4B-E). In contrast, the morphology of nestin-positive radial precursors, including their basal processes, was apparently

similar in *Ankrd11*$^{Yod/+}$ and wildtype cortices (Figure S4A,B).

To extend this analysis, we crossed male *Ankrd11*$^{Yod/+}$ mice with wildtype females, injected pregnant mothers with BrdU at gestational day 13.5, and immunostained sections 5 days later. BrdU-positive cells were mislocalized in Yoda cortices (Figure 4G). We quantified this, using similarly-aged wildtype and Yoda sections triple-labelled for Satb2, Pax6 and the intermediate progenitor marker Tbr2 to define the cortical regions (Figures 4F and S4C). This analysis showed significantly more BrdU-positive cells in the *Ankrd11*$^{Yod/+}$ IZ and fewer in the CP (Figure 4H). Double-labeling also showed significantly fewer BrdU-positive, Ki67-positive precursors in the VZ/SVZ (Figures 4I and K), and fewer total BrdU-positive, Satb2-positive cells (Figures 4J, 4L and S4D) in *Ankrd11*$^{Yod/+}$ cortices. These changes were not due to cell senescence, as monitored by SA-β-gal staining (data not shown). Thus, as seen with acute *Ankrd11* knockdowns, a heterozygous Yoda mutation caused decreased precursor proliferation, and perturbed genesis and localization of neurons.

Ankrd11$^{Yod/+}$ *mice have perturbations in adult neural precursors, and are behaviorally abnormal*

We asked whether adult neural precursor cells (NPCs) from *Ankrd11*$^{Yod/+}$ mice were also perturbed, initially focusing on the adult SVZ. We injected adult wildtype and *Ankrd11*$^{Yod/+}$ mice with BrdU and immunostained SVZ sections 24 hours later. *Ankrd11*$^{Yod/+}$ mice had significantly fewer BrdU-positive SVZ cells and fewer Sox2-positive NPCs that were BrdU-positive (Figures 5A-C). We also asked about adult-born olfactory bulb neurons by immunostaining olfactory bulb sections one month following multiple BrdU injections. Adult-born BrdU-positive, NeuN-positive olfactory bulb neurons were significantly reduced in *Ankrd11*$^{Yod/+}$ mice (Figures 5D,E).

We also examined the other adult NPC niche, the subgranular zone (SGZ) of the dentate gyrus, by analyzing hippocampal sections 24 hours following BrdU injection. The *Ankrd11*$^{Yod/+}$ SGZ contained fewer BrdU-positive cells, Sox2-positive cells, and double-labelled BrdU-positive, Sox2-positive proliferating NPCs (Figures 5F-H and S5A). Doublecortin-positive neuroblasts and newborn neurons were also reduced in the *Ankrd11*$^{Yod/+}$ SGZ (Figures 5I and S5B). We also asked about mature adult-born neurons, administering BrdU and immunostaining hippocampal sections one month later (Figure S5C). BrdU-positive, NeuN-positive adult-born

neurons in the dentate gyrus were significantly decreased in *Ankrd11*$^{Yod/+}$ mice (Figure 5J). Thus, Ankrd11 is also important for adult NPC proliferation and neurogenesis.

Since *ANKRD11* mutations are associated with intellectual disability and ASD in humans, we characterized the Yoda mice behaviorally. Initially, we used the open field test to ask about general levels of activity. *Ankrd11*$^{Yod/+}$ mice travelled significantly less distance in the open field than their wildtype counterparts (Figure 5K). This decrease was due to a reduction in total time spent traveling (400.73 +/- 25.2 seconds for *Ankrd11*$^{Yod/+}$ versus 478.9 +/- 22.8 for wildtypes, $p = 0.03$) rather than a change in movement velocity, which was similar for both groups (33.7 +/- 1.15 cm/second for *Ankrd11*$^{Yod/+}$ and 35.8 +/- 1.12 cm/second for wildtypes; $p > 0.05$).

We then tested the *Ankrd11*$^{Yod/+}$ mice in a three chamber social preference test (Moy et al., 2004) that assays social interactions with an unfamiliar mouse, a behavior that is perturbed in some mouse models of ASD (Crawley et al., 2007; Molina et al., 2008; Carter et al., 2011). To perform this test, mice were placed in and allowed to habituate to a three chamber environment; wildtype and *Ankrd11*$^{Yod/+}$ mice spent equivalent percentages of time in each of the compartments during this habituation ($p > 0.05$). We then put an unfamiliar mouse (stranger 1 [Str1]) in one of the chambers. As predicted, wildtype mice spent more time in the chamber side containing the unfamiliar mouse relative to that containing an inanimate target (Emt) (Figure 5L). In contrast, *Ankrd11*$^{Yod/+}$ mice showed no significant preference (Figure 5L). Similar results were obtained whether the unfamiliar mouse was placed in chamber 1 or chamber 3 ($p > 0.05$).

We then asked whether the mice would prefer a new unfamiliar mouse over the now-familiar stranger 1 mouse by replacing the inanimate object with a second stranger mouse (stranger 2 [Str2]). Wild type mice spent significantly more time in the chamber containing stranger 2 than in that containing stranger 1. In contrast, the *Ankrd11*$^{Yod/+}$ mice did not prefer the stranger 2 mouse (Figures 5M and 5N).

We then assayed repetitive behaviors, which are thought to be ASD-like, by measuring self-grooming (Carter et al., 2011). Mice were placed into a cage for one hour to habituate, and were then observed for 10 minutes. Over this period, *Ankrd11*$^{Yod/+}$ mice spent twice as much time grooming themselves as did their wildtype littermates (Figure 5O). Thus, *Ankrd11*$^{Yod/+}$ mice display behaviors that could reflect cognitive dysfunction and ASD-like perturbations.

Perturbations in Ankrd11 cause global changes in gene expression in cortical precursors

To ask if Ankrd11 is a transcriptional coregulator, we compared gene expression in neural precursors from embryonic Yoda versus wildtype mice. To do so, we expanded E14 cortical precursors as neurospheres for 6 days in EGF and FGF2, and then passaged and expanded these as secondary neurospheres for analysis. Simultaneously, we grew the same cells at clonal density for quantification. The clonal analysis showed that the *Ankrd11*$^{Yod/+}$ embryonic cortex contained only about half as many neurosphere-initiating cells (Figure 6A). Moreover, these were decreased in their ability to self-renew, since fewer secondary spheres were generated when they were passaged at clonal density (Figure 6B), confirming that Ankrd11 is required for cortical precursor self-renewal.

We analyzed the transcriptome of the expanded secondary neurospheres by microarray, comparing six and five biological replicates of *Ankrd11*$^{Yod/+}$ and wildtype neurospheres, respectively, with the Affymetrix GeneChip Mouse Gene 2.0 Array (GEO accession #GSE63303). Spearman rank correlation (Figure 6C) showed that these two populations differed at the transcriptome level. In addition, while the wildtype neurosphere samples were all relatively similar to each other, the *Ankrd11*$^{Yod/+}$ neurospheres showed more heterogeneity, potentially due to variable penetrance of the heterozygote phenotype (Figure 6C).

To further investigate these differences, we performed differential expression analysis to compare the wildtype and *Ankrd11*$^{Yod/+}$ datasets using the Parteks Genomic Suite. 761 genes, or approximately 3% of those analyzed, were significantly differentially expressed (using FDR p-value < 0.1 and FC > 1.1 or < -1.1) (Figure 6D and Table S1). These genes clearly distinguished the *Ankrd11*$^{Yod/+}$ and wildtype precursors, as shown in a heatmap (Figure 6E). We validated these results by real-time quantitative PCR (qPCR), confirming mRNAs that were upregulated (*Notch1*, *Slc1A2*, *Mll5*, *Fzd3*, *Sox6*, *Ncor1*, *Foxn3, Med13* and *Ncoa1*), or downregulated (*Eya2*, *Med10*, *Foxp1* and *Gabrg1*) in *Ankrd11*$^{Yod/+}$ neurospheres. This analysis validated the microarray data (Figure 6F), showing a Pearson correlation coefficient of 0.995 (Figure 6G).

We then subjected the 761 differentially expressed genes to gene ontology and pathway analysis. This analysis showed that the enriched pathways were diverse in terms of their functions (Figure 6H and Table S2). Intriguingly, two disorder categories with the highest p-

values were schizophrenia and abnormal morphology of the nervous system (Figure 6H), consistent with the phenotypes that we observed in the Yoda mice.

Ankrd11 associates with chromatin and histone acetylation is increased in Ankrd11$^{Yod/+}$ neural precursors

Since Ankrd11 can bind HDACs, we asked whether chromatin acetylation was altered in Yoda mice, initially isolating total histones from adult *Ankrd11$^{Yod/+}$* and wildtype cortices. Western blots demonstrated increased acetylation of histones H3 and H4 at H3K9, H4K5, H4K8, and H4K16 (Figure 7A), all known HDAC3 target sites (Rudenko and Tsai, 2014). We then examined histone acetylation in the E14 cortical neurospheres used for the microarrays. Western blots showed that, relative to total histone H4, acetylation in the *Ankrd11$^{Yod/+}$* neurosphere chromatin was increased at H4K5, H4K8, H4K16 and H3K9, but unaltered at H3K14 and H3K27 (Figures 7B,C).

To ask if altered histone acetylation could explain the observed gene expression changes, we analyzed H4K16 acetylation on genes upregulated in *Ankrd11$^{Yod/+}$* neurospheres, focusing on *Notch1*, *Slc1A2*, *Mll5*, *Fzd3*, *Sox6* and *Ncor1*. To do so, we immunoprecipitated cortical neurosphere chromatin with anti-H4K16ac or anti-H4, and analysed genomic elements located within 1 kb of the 5'UTR by qPCR, focusing on sequences associated with acetylated H3K27 in E14.5 whole brain (ENCODE database, GEO accession #GSM1000094) (Rosenbloom et al., 2013). This analysis showed that, in *Ankrd11$^{Yod/+}$* neurospheres, H4K16 acetylation was significantly increased on the *Notch1*, *Slc1A2*, *Mll5, Fzd3* and *Sox6* genomic elements (Figure 7D).

To ask if these genomic loci were direct targets of Ankrd11, we performed ChIP with anti-Ankrd11. Since the *p21* gene is directly regulated by Ankrd11 (Neilsen et al., 2008), we initially validated the Ankrd11 antibody for ChIP with the *p21* promoter (Neilsen et al., 2008). This analysis showed that anti-Ankrd11 immunoprecipitates were significantly enriched for the *p21* gene element relative to non-specific IgG and to the desert region on chromosome 15, which is at least 500 kbp away from any known gene (Figure S6A). We then performed ChIP for the selected genes in wildtype neurospheres. Ankrd11 was significantly associated with *Notch1*, *Slc1A2, Mll5*, *Fzd3*, *Sox6* and *Ncor1* gene elements, but not with *Foxn3*, *Med10* or *Ncoa1* gene elements (Figure 7E). Importantly, none of these latter gene elements showed significantly

altered H4K16 acetylation in *Ankrd11*$^{Yod/+}$ neurospheres ($p>0.06$; data not shown).

Ankrd11 controls neural precursor proliferation via HDAC3 and histone acetylation

The strong correspondence between Ankrd11 chromatin association sites, and increased H4K16 acetylation at those sites in *Ankrd11*$^{Yod/+}$ neurospheres suggests that Ankrd11 directly regulates HDAC function. To test this idea, we focused on HDAC3 which interacts with Ankrd11 when overexpressed (Zhang et al., 2004). Immunostaining of cultured precursors showed that HDAC3 was present in some Ankrd11-positive nuclear foci (Figure 7F). To ask if they directly associated, we performed proximity ligation assays (PLA), which provide a positive readout when antibody targets are within 40 nm of each other (Soderberg et al., 2006). Bright fluorescent nuclear puncta were observed when anti-Ankrd11 and anti-HDAC3 were combined, but not when anti-eIF4E, which robustly immunostains cortical precursors (Yang et al., 2014) was combined with either anti-Ankrd11 or anti-HDAC3 (Figures 7G and S6B).

These data identify an Ankrd11/HDAC3 complex in cortical precursors, and suggest that Ankrd11 mutation or knockdown disrupts this complex and thus abnormally elevates histone acetylation. We therefore asked whether rebalancing histone acetylation with the HAT inhibitor C646 (Bowers et al., 2010) would rescue the *Ankrd11* knockdown-induced changes, focusing on precursor proliferation. Cultured precursors were transfected with EGFP and control or *Ankrd11* shRNA, were treated with 500 nM C646 after 1 day, and stained for Ki67 2 days later. C646 completely rescued the reduced proliferation seen following *Ankrd11* knockdown (Figure 7H).

Finally, we asked whether ectopic HDAC3 expression could also rescue this proliferation phenotype. Cultured precursors were cotransfected with EGFP and *Ankrd11* shRNA with or without an *HDAC3* expression plasmid. Immunostaining 3 days later demonstrated that HDAC3 had no effect on Ki67-positive cells under basal conditions, but that it completely rescued the decreased proliferation caused by *Ankrd11* knockdown (Figure 7I).

DISCUSSION

ASD is a constellation of behaviorally-related neurodevelopmental disorders with a strong genetic component. Many genes have been associated with ASD, and one key question is how they cause ASD-type behaviors. In this regard, a subset of these genes regulates synaptogenesis, but a further subset has no identified function in the brain. Here, we have focused upon one of the latter genes encoding a nuclear protein, Ankrd11, that has been implicated as a transcriptional coregulator. Individuals with *ANKRD11* mutations display neurodevelopmental phenotypes, including aspects of ASD, cognitive disability (Sirmaci et al., 2011; Lo-Castro et al., 2013; Iossifov et al., 2014), and neuroanatomical perturbations such as periventricular heterotopias (Willemsen et al., 2010) Here, we show that Ankrd11 plays an important role during neural development, acting to determine appropriate histone acetylation and gene expression and thus proliferation of embryonic neural precursors and the genesis and positioning of newborn neurons. Moreover, we show that disruption of Ankrd11 causes long-lasting changes in the adult forebrain together with ASD-like behaviors, thereby providing an explanation for the perturbations that occur when *ANKRD11* is mutated in humans.

How does Ankrd11 regulate neural development? We propose it functions as a transcriptional coregulator that binds to HDAC3 and potentially other HDACs, and in so doing regulates histone acetylation, gene expression and ultimately the biology of developing precursors and neurons. This model is based upon previous work in cell lines together with data here showing that (a) HDAC3 and Ankrd11 colocalized and associated in cortical precursors, (b) histone acetylation was increased and gene expression broadly perturbed in Yoda cortical precursors, (c) for some genes, this increased histone acetylation and gene expression correlated with Ankrd11 chromatin association, and (d) rebalancing histone acetylation by overexpression of HDAC3 or pharmacological HAT inhibition rescued the *Ankrd11* knockdown-mediated decrease in precursor proliferation. This model is consistent with previous studies showing that disruption of HDAC3 altered neural precursor proliferation and neuronal differentiation (Sun et al., 2007; Castelo-Branco et al., 2014), and caused increased H4K8 acetylation coincident with changes in neuronal gene expression (McQuown et al., 2011), phenotypes that are reminiscent of those seen following disruption of Ankrd11.

A number of additional intriguing conclusions came from the Yoda cortical precursor gene expression analyses. First, the type of genes that were deregulated in Yoda precursors was

diverse, suggesting that Ankrd11 likely plays a relatively global role as a transcriptional coregulator. Many of these deregulated genes encode known regulators of cortical development, including transcriptional or chromatin regulators such as *SOX6*, *RelA*, *RB1*, *Notch1*, *NCOA1*, *NCOR1, NCOR2*, *MLL5*, *ARID2*, *MED10*, *MED13*, *WDR61*, *WDR26*, *FOXP1*, *ZEB2*, *ATF5*, *EYA2*, and *FOXN3*, and signaling molecules such as *PTCH1*, *DCC*, *SEMA5B*, *FZD3*, and, *SPRY1* (see Table S1). Our ChIP studies indicate that at least a subset of these genes are directly associated with Ankrd11. Thus, Ankrd11 may coordinately regulate multiple genes important for neural development by modulating or fine-tuning their expression. Second, one robust disease association for the deregulated genes was schizophrenia. Since many genes implicated in ASD are also associated with schizophrenia (Mullin et al., 2013; McCarthy et al., 2014), then our finding that mutation of an ASD-associated gene caused changes in genes implicated in schizophrenia supports the idea of a common cellular network.

Our data show that Yoda mice, like humans carrying one mutant *ANKRD11* allele, exhibit neuroanatomical perturbations such as neurons misplaced around the lateral ventricles (periventicular heterotopias), and ASD-like behaviors. These findings are intriguing in light of the recent description of patches of cortical disorganization in children with autism (Stoner et al., 2014), and support the idea that the Yoda mouse is a model for the human situation. However, these findings also raise the possibility that there are multiple mechanisms that can lead to ASD-like behavior, both in mice and humans. While one likely mechanism involves later aspects of circuit formation like synaptogenesis, our findings suggest a second important mechanism involving early changes in neurogenesis and neuronal specification/localization that ultimately provide an aberrant template upon which to build the circuitry that is essential for normal cognitive function.

EXPERIMENTAL PROCEDURES

Animals and genotyping. All animal use was approved by the HSC Animal Care Committee in accordance with CCAC policies. *Ankrd11*$^{yod/+}$ mice (Barbaric et al., 2008) were from the European Mouse Mutant Archive (EMMA) and genotyped as in Suppl. Procedures. CD1 mice (Charles River) were used in all other experiments.

Plasmids and shRNAs. We used previously-published plasmids, pEF-EGFP , PCAG-PB-EGFP and PCAG-Pbase (Gallagher et al., 2013). The *HDAC3* plasmid (Origene) was in the pCMV6 backbone and *Ankrd11* shRNAs (EZ Biolabs) were in the pGCsi backbone. shRNA sequences are in Suppl. Procedures.

Cell cultures. E12.5 cortical precursors were cultured and transfected at 125,000 - 150,000 cells/ml as described (Barnabé-Heider et al., 2005). E14 cortical neurospheres were cultured and passaged at 6 days under standard conditions at 50 cells/μl for biochemistry and clonal density (Coles-Takabe et al., 2008) for quantification, counting spheres with at least 10 cells. For human precursors, Hes2 ES cells were differentiated as described (Wang et al., 2012). HEK 293 cells and NIH/3T3 cells were cultured as described (Zander et al., 2014). Additional details are in Suppl. Procedures.

In utero electroporations and BrdU experiments. *In utero* electroporations and embryonic BrdU experiments were performed as described (Zander et al., 2014). For adult BrdU studies, 6 month-old mice were injected once with 100 mg/Kg BrdU or 5 times with 60 mg/kg BrdU and analyzed 24 hours or 30 days later, respectively, by counting 10 SVZ, dentate gyrus or olfactory bulb sections, sampled every tenth section, as described (Cancino et al., 2013) and detailed in Suppl. Procedures.

Immunocytochemistry, proximity ligation assays, microscopy, and quantification. Immunocytochemistry of cultured cells and cryopreserved or paraffin-embedded tissue was performed as described (Cancino et al., 2013; Zander et al., 2014). Proximity ligation assays were carried out using Duolink in situ red starter kit for mouse/rabbit as per manufacturers instructions (Sigma-Aldrich). For culture knockdowns or for clonal analysis, over 100

transfected cells or clones per condition per experiment were quantified. For Ankrd11 expression levels, Northern Eclipse (Empix) software was used to determine signal over a threshold level. For *in vivo* analysis, coronal sections were analyzed using a Zeiss Pascal confocal microscope. Four sections/embryo were analyzed, taking three pictures covering the VZ, SVZ, IZ and CP of sections at equivalent anatomic levels.

qRT-PCR and microarrays. RNA and cDNA preparation, primers and qRT-PCR methods are in Suppl. Procedures. For microarrays 5.5 μg of cDNA was hybridized to the Affymetrix Gene Chip Mouse Gene 2.0 ST and results analyzed using Partek Genomics Suite 6.6. Only probesets for annotated genes were used for differential expression analysis. ANOVA statistics were calculated and the genes with false discovery (FDR) p-value < 0.1 and fold change (FC) > 1.1 or < -1.1 were considered statistically significant. Affymetrix Expression Console 1.1 was used for Spearman rank correlations, Partek Genomics Suite 6.6 for unbiased hierarchical clustering and heatmaps, and Ingenuity Pathway Analysis (IPA, version 18488943) for gene ontology pathways. Microarray data can be found at GEO accession #GSE63303.

Chromatin preparations and immunoprecipitation (ChIP) analysis. Chromatin from secondary passage neurospheres was prepared as described (Savage et al., 2009; Suppl. Procedures). ChIP was performed as described (Savage et al., 2009) with 20 μg chromatin and 4 μg anti-Ankrd11 (Neilsen et al. 2008) or non-specific rabbit IgG (Millipore), or 2 μg chromatin and 2 μg anti-H4 or anti-H4K16ac (Millipore). Chromatin was reverse-crosslinked, DNA purified, and Ankrd11-, H4K16ac- and total H4-bound chromatin calculated as percent input by qPCR with primers listed in Suppl. Procedures. To be considered a true association, enrichment with a specific antibody was compared to non-specific IgG ($p<0.05$). All primers were validated and qPCR assays were performed in accordance with MIQE guidelines.

***Western blots and densitometry*.** Westerns for proteins other than histones were performed as described (Barnabé-Heider et al., 2005). For cortical histones, tissue was dissected in PBS plus 5 mM sodium butyrate to retain acetylation, and histones were extracted and analyzed as described in Suppl. Procedures. For neurospheres, 1 μg chromatin was reverse-crosslinked at 65°C for 16 hours, incubated at 95°C in Laemmli sample buffer for 10 minutes and analyzed on western

blots. Images were captured using MicroChemi4.2 imaging system (DNR Bio-imaging Systems), and densitometry performed using GelQuant software (DNR Bio-imaging Systems). Background was subtracted using the rolling ball method and densities were normalized to total H4 and expressed over one of the wildtype samples (equated to "1"). Antibodies are in Suppl. Procedures.

Behavioral Analyses. Mice were tested at 10 weeks of age, and their behavior assessed as in Suppl. Procedures.

Statistics: All data other than the microarray were expressed as mean plus or minus the standard error of the mean (SEM), and tested for significance with Student's *t*-tests unless otherwise indicated, in which case they were analyzed with an ANOVA with Fisher's post-hoc test or by two way repeated measures ANOVA (genotype X side) with Bonferroni 's post hoc test.

Author Contributions

D.G. conceptualized and performed the phenotypic experiments, and analyzed data and co-wrote the paper. A.V. conceptualized, performed and analysed the gene expression, histone acetylation and ChIP experiments and co-wrote the paper. M.A.Z. performed revisions and co-wrote the paper. G.I.C. performed adult neurogenesis experiments. A.B. performed initial Ankrd11 expression studies. M.P.K. participated in gene expression analyses. C.A. performed behavioral analyses. M.T. cosupervised the behavioral studies. P.M.N. and D.F.C. provided antibodies and plasmids. S.W.S. provided intellectual input and unpublished data. G.M.K. supervised the human pluripotent cell work. K.W. supervised, conceptualized and analyzed the behavioral experiments. D.R.K. and F.D.M. conceptualized and analyzed all experiments other than behavioral, and co-wrote the manuscript. All authors read and contributed to the manuscript.

Acknowledgements

This work was funded by CIHR grant MOP-125945, a Brain Canada MIRI grant, and by the Three to Be Foundation. FDM is an HHMI Senior International Research Scholar, and FDM and DRK are CRC chairholders. SWS holds the GlaxoSmithKline-CIHR Chair in Genome Sciences. DG was funded by a McEwen Center McMurrich fellowship, AV by fellowships from the MS Society of Canada, CIHR, and Hospital for Sick Children, MPK by a CIHR fellowship, and GIC by a Heart and Stroke Foundation fellowship. We would particularly like to thank Martin Fray (MRC, Harwell) and the European Mutant Mouse Archive for help with the Yoda mice. We also thank Sarah Burns and Dennis Aquino for important technical assistance, and Lisa Julian and Cheryl Arrowsmith for valuable advice.

REFERENCES

Barbaric, I., Perry, M.J., Dear, T.N., Rodriguez Da Costa, A., Salopek, D., Marusic, A., Hough, T., Wells, S., Hunter, A.J., Cheeseman, M., and Brown, S.D.M. (2008). An ENU-induced mutation in the Ankrd11 gene results in an osteopenia-like phenotype in the mouse mutant Yoda. Physiol. Genomics *32*, 311-321.

Barnabé-Heider, F., Wasylnka, J.A., Fernandes, K.J., Porsche, C., Sendtner, M., Kaplan, D.R., and Miller, F.D. (2005). Evidence that embryonic neurons regulate the onset of cortical gliogenesis via cardiotrophin-1. Neuron *48*, 253-65.

Bowers, E.M., Yan, G., Mukherjee, C., Orry, A., Wang, L., Holbert, M.A., Crump, N.T., Hazzalin, C.A., Liszcazk, G., Yuan, H., et al. (2010). Virtual ligand screening of the p300/CBP histone acetyltransferase: identification of a selective small molecule inhibitor. Chem. Biol. *17*, 471-482.

Cancino, G.I., Yiu, A.P., Fatt, M.P., Dugani, C.B., Flores, E.R., Frankland, P.W., Josselyn, S.A., Miller, F.D., and Kaplan, D.R. (2013) p63 Regulates Adult Neural Precursor and Newly Born Neuron Survival to Control Hippocampal-Dependent Behavior. J. Neurosci. *33*, 12569–12585.

Carter, M.D., Shah, C.R., Muller, C.L., Crawley, J.N., Carneiro, A.M., and Veenstra-VanderWeele, J. (2011). Absence of preference for social novelty and increased grooming in integrin β3 knockout mice: initial studies and future directions. Autism Res. *4*, 57-67.

Castelo-Branco, G., Lilja, T., Wallenborg, K., Falcão, A.M., Marques, S.C., Gracias, A., Solum, D., Paap, R., Walfridsson, J., Teixeira, A.I. et al. (2014) Neural stem cell differentiation is dictated by distinct actions of nuclear receptor corepressors and histone deacetylases. Stem Cell Rep. *3*, 502-15.

Coles-Takabe, B.L., Brain, I., Purpura, K.A., Karpowicz, P., Zandstra, P.W., Morshead, C.M., and van der Kooy, D. (2008). Don't look: growing clonal versus nonclonal neural stem cell colonies. Stem Cells. *11*, 2938-44.

Crawley, J.N., Chen, T., Puri, A., Washburn, R., Sullivan, T.L., Hill, J.M., Young, N.B., Nadler, J.J., Moy, S.S., Young, L.J. et al. (2007). Social approach behaviors in oxytocin knockout mice: comparison of two independent lines tested in different laboratory environments. Neuropeptides *41*, 145-163.

Devlin, B., and Scherer, S. (2012). Genetic architecture in autism spectrum disorder. Curr. Opin. Genet. Dev. *22*, 229-237.

Gallagher, D., Norman, A.A., Woodard, C.L., Yang, G., Gauthier-Fisher, A., Fujitani, M., Vessey, J.P., Cancino, G.I., Sachewsky, N., Woltjen, K., Fatt, M.P., Morshead, C.M., Kaplan, D.R., and Miller, F.D. (2013). Transient maternal IL-6 mediates long-lasting changes in neural stem cell pools by deregulating an endogenous self-renewal pathway. Cell Stem Cell *13*, 564-576.

Iossifov, I. et al. (2014). The contribution of de novo coding mutations to autism spectrum disorder. Nature, doi:10.1038/nature13908.

Jamain, S., Radyushkin, K., Hammerschmidt, K., Granon, S., Boretius, S., Varoqueaux, F., Ramanantsoa, N., Gallego, J., Ronnenberg, A., Winter, D. et al. (2008). Reduced social interaction and ultrasonic communication in a mouse model of monogenic heritable autism. Proc. Natl. Acad. Sci. *105*, 1710-1715.

Li, C.W., Dinh, G.K., Zhang, A., and Chen, J.D. (2008). Ankyrin repeats-containing cofactors interact with ADA3 and modulate its co-activator function. Biochem. J. *413*, 349-357.

Lilja, T., Heldring, N., and Hermanson, O. (2013). Like a rolling histone: epigenetic regulation of neural stem cells and brain development by factors controlling histone acetylation and methylation. Biochim. Biophys. Acta *1830*, 2354-2360.

Lo-Castro, A., Brancati, F., Digilio, M.C., Garaci, F.G., Bollero, P., Alfieri, P., and Curatolo, P. (2013) Neurobehavioral phenotype observed in KBG syndrome caused by ANKRD11 mutations. Am. J. Med. Genet. B. Neuropsychiatr. Genet. *162B,* 17-23.

Marshall, C.R. et al. (2008). Structural variation of chromosomes in autism spectrum disorder. Am. J. Hum. Genet. *82*, 477-488.

McCarthy, S.E., Gillis, J., Kramer, M., Lihm, J., Yoon, S., Berstein, Y., Mistry, M., Pavlidis, P., Solomon, R., Ghiban, E. et al. (2014). De novo mutations in schizophrenia implicate chromatin remodeling and support a genetic overlap with autism and intellectual disability. Mol Psychiatry. *19*, 652-8.

McQuown, S.C., Barrett, R.M., Matheos, D.P., Post, R.J., Rogge, G.A., Alenghat, T., Mullican, S.E., Jones, S., Rusche, J.R., Lazar, M.A., and Wood, M.A. (2011). HDAC3 is a critical negative regulator of long-term memory formation. J. Neurosci. *31*, 764-74.

Molina, J., Carmona-Mora, P., Chrast, J., Krall, P.M., Canales, C.P., Lupski, J.R., Reymond, A., and Walz, K. (2008). Abnormal social behaviors and altered gene expression rates in a mouse model for Potocki-Lupski syndrome. Hum. Mol. Genet. *17*, 2486-2495.

Moy, S.S., Nadler, J.J. Perez, A., Barbaro, R.P., Johns, J.M., Magnuson, T.R., Piven, J., and Crawley, J.N. (2004). Sociability and preference for social novelty in five inbred strains: an approach to assess autistic-like behavior in mice. Genes Brain Behav. *3*, 287-302.

Mullin, A.P., Gokhale, A., Moreno-De-Luca, A., Sanyal, S., Waddington, J.L., and Faundez, V. (2013). Neurodevelopmental disorders: mechanisms and boundary definitions from genomes, interactomes and proteomes. Transl Psychiatry. *3*, e329.

Neilsen, P.M., Cheney, K.M., Li, C.W., Chen, J.D., Cawrse, J.E., Schulz, R.B., Powell, J.A., Kumar, R., and Callen, D.F. (2008). Identification of ANKRD11 as a p53 coactivator. J. Cell Sci. *121*, 3541-3552.

Pinto, D. et. al. (2014). Convergence of genes and cellular pathways dysregulated in autism spectrum disorders. Am. J. Hum. Genet. *94*, 677-694.

Rosenbloom, K.R., Sloan, C.A., Malladi, V.S., Dreszer, T.R., Learned, K., Kirkup, V.M., Wong, M.C., Maddren, M., Fang, R., Heitner, S.G. et al. (2013) ENCODE data in the UCSC Genome Browser: year 5 update. Nucleic Acids Res. *41*, D56-63.

Rudenko, A., and Tsai, L.H. (2014). Epigenetic modifications in the nervous system and their impact upon cognitive impairments. Neuropharmacol. *80*, 70-82.

Savage, J., Conley, A.J., Blais, A., and Skerjanc, I.S. (2009). SOX15 and SOX7 differentially regulate the myogenic program in P19 cells. Stem Cells. *27*, 1231-43.

Sirmaci, A., Spiliopoulos, M., Brancati, F., Powell, E., Duman, D., Abrams, A., Bademci, G., Agolini, E., Guo, S., Konuk, B. et al. (2011). Mutations in ANKRD11 cause KBG syndrome, characterized by intellectual disability, skeletal malformations, and macrodontia. Am. J. Hum. Genet. *89*, 289-294.

Soderberg, O., Gullberg, M., Jarvius, M., Ridderstrale, K,, Leuchowius, K.J., Jarvius, J., Wester, K., Hydbring, P., Bahram, F., Larsson, L.G., and Landegren, U. (2006) Direct observation of individual endogenous protein complexes in situ by proximity ligation. Nat.Methods *3*, 995-1000.

Stoner, R., Chow, M.L., Boyle, M.P., Sunkin, S.M., Mouton, P.R., Roy, S., Wynshaw-Boris, A., Colamarino, S.A., Lein, E.S. and Courchesne, E. (2014). Patches of disorganization in the neocortex of children with autism. N. Engl. J. Med. *370*, 1209-1219.

Sun, G., Yu, R.T., Evans, R.M., and Shi Y. (2007). Orphan nuclear receptor TLX recruits histone deacetylases to repress transcription and regulate neural stem cell proliferation. Proc. Natl. Acad. Sci. *104*, 15282-15287.

Tsui, D., Vessey, J.P., Tomita, H., Kaplan, D.R., and Miller, F.D. (2013) FoxP2 regulates embryonic cortical neurogenesis. J. Neurosci. *33*, 244-258.

Wang, J., Weaver, I.C., Gauthier-Fisher, A., Wang, H., He, L., Yeomans, J., Wondisford, F., Kaplan, D.R., and Miller, F.D. (2009). CBP histone acetyltransferase activity regulates embryonic neural differentiation in the normal and Rubinstein-Taybi syndrome brain. Dev. Cell *18*, 114-25.

Wang, J., Gallagher, D., DeVito, L.M., Cancino, G.I., Tsui, D., He, L., Keller, G.M., Frankland, P.W., Kaplan, D.R., and Miller, F.D. (2012). Metformin activates an atypical PKC-CBP pathway to promote neurogenesis and enhance spatial memory formation. Cell Stem Cell *11*, 23-35.

Willemsen, M.H., Fernandez, B.A., Bacino, C.A., Gerkes, E., de Brouwer, A.P., Pfundt, R., Sikkema-Raddatz, B., Scherer, S.W., Marshall, C.R., Potocki, L., van Bokhoven, H., and Kleefstra, T. (2010). Identification of ANKRD11 and ZNF778 as candidate genes for autism and variable cognitive impairment in the novel 16q24.3 microdeletion syndrome. Eur. J. Hum. Genet. *18*, 429-435.

Yang, G., Smibert, C.A., Kaplan, D.R., and Miller, F.D. (2014) An eIF4E/4E-T complex determines the genesis of neurons from precursors by translationally repressing a proneurogenic transcription program. Neuron (in press).

Zander M.A., Burns S.E., Yang G., Gridley T., Kaplan D.R., and Miller F.D. (2014). Snail coordinately regulates conserved downstream pathways to control multiple aspects of mammalian neural precursor biology. J. Neurosci. *34*, 5164-5175.

Zhang, A., Li, C.-W., and Chen, J.D. (2007a). Characterization of transcriptional regulatory domains of ankyrin repeat cofactor-1. Biochem. Biophys. Res. Commun. *358*, 1034-1040.

Zhang, A., Li, C.W., Tsai, S.C., and Chen, J.D. (2007b). Subcellular localization of ankyrin repeats cofactor-1 regulates its corepressor activity. J. Cell. Biochem. *101*, 1301-1315.

Zhang, A., Yeung, P.L., Li, C.-W., Tsai, S.-C., Dinh, G.K., Wu, X., Li, H., and Chen, J.D. (2004). Identification of a novel family of ankyrin repeats containing cofactors for p160 nuclear receptor coactivators. J. Biol. Chem. *279*, 33799-33805.

FIGURE LEGENDS

Figure 1. ***Ankrd11 is expressed in murine embryonic cortical precursors and regulates their proliferation and differentiation in culture.*** (A) Quantitative RT-PCR for *Ankrd11* mRNA relative to *GAPDH* mRNA in the E12 to P3 cortex. (B) Western blot of Ankrd11 in E11 to P3 cortex. The blot was reprobed for p130cas as a loading control. (C-E) Images of E12 (C) or E16 (D,E) cortical sections immunostained for Ankrd11 (red) and Pax6 (D, green) or βIII-tubulin (E, green), counterstained with Hoechst 33258 (blue) to highlight nuclei. The right panels show higher magnification images of the VZ (C; arrows denote Ankrd11-positive nuclear foci) or boxed areas (D,E). (F) Western blot for Ankrd11 in NIH/3T3 cells transfected with control (Con) or one of two *Ankrd11* shRNAs (sh1 or sh2). The blot was reprobed for p130cas. (G) E12.5 cortical precursors cultured 3 days and immunostained for Ankrd11 (red) and Ki67, Pax6 or βIII-tubulin (all green). Arrows denote double-positive cells. (H,I) Precursors were cotransfected with EGFP and control (Con) or *Ankrd11* shRNA (sh1 or sh2), immunostained for EGFP (green) and Ankrd11 (red) 2 days later (H) and EGFP-positive cells expressing detectable Ankrd11 quantified by fluorescence intensity (I). (H) shows cells transfected with *Ankrd11* sh2, and the arrow and arrowhead denote EGFP-positive, Ankrd11-negative, and EGFP-negative, Ankrd11-positive cells, respectively. $^{**}p < 0.01$, $^{***}p < 0.005$, n = 3 experiments. (J-P) E12.5 precursors were cotransfected with nuclear EGFP, and control (Con) or *Ankrd11* shRNA (sh1 or sh2), and analyzed 2 or 3 days later. (J,K) Cells immunostained for EGFP (green, J) and Ki67 (red, J) after 2 days and quantified (K). Arrow denotes a double-positive cell. $^{**}p < 0.01$, n = 4 experiments. (L) EGFP-positive precursors that were BrdU-positive when cultures were exposed to BrdU after 1 day, and analyzed 2 days later. $^{**}p < 0.01$, n = 3 experiments. (M-P) Cultures were immunostained for EGFP (green, M) and Pax6 or βIII-tubulin (red, M) at 3 days and quantified (N,P) for double-labelled cells (arrows in M). (O) shows the percentage of EGFP-positive, Pax6-positive cells that were also Ki67-positive, as calculated from (K) and (N). $^{*}p < 0.05$, $^{**}p < 0.01$, n = 3 or 4 experiments. Scale bars, (C) = 100 μm, (D,E) = 20 μm, (G,H,J,M, inset in C) = 10 μm. Error bars indicate standard error of the mean (S.E.M.). **See also Figure S1.**

Figure 2. ***Knockdown of Ankrd11 in cultured murine or human cortical precursors or in the murine embryonic cortex perturbs proliferation and neurogenesis*.** (A-E) E12.5 precursors were cotransfected with the PB transposase and PB-EGFP reporter, and control (Con) or

Ankrd11 shRNA (sh2), immunostained for EGFP (green, A), Sox2 (red, A) and βIII-tubulin (purple, A) after 3 days, and quantified for clones greater than one cell in size (B), neuron-only clones (C), clones with at least one Sox2-positive precursor (D), and number of Sox2-positive cells in clones with at least one Sox2-positive precursor (E). Arrows in (A) denote EGFP-positive, Sox2-positive precursors. *$p < 0.05$, n = 3 experiments. (F) ES cell-derived human cortical precursors immunostained for Ankrd11 (red) and Ki67 or βIII-tubulin (green). Arrows denote double-positive cells. (G) Western blot of Ankrd11 in HEK293 cells transfected with control (Con) or human *Ankrd11* shRNA (sh3), analyzed after 24 hours. The blot was reprobed for p130cas. (H-K) Human cortical precursors were cotransfected with EGFP and control (Con) or human-specific *Ankrd11* shRNA (sh3), immunostained 3 days later for EGFP (green, I), and Ankrd11, Ki67 (red, I) or βIII-tubulin (red, I) and quantified for EGFP-positive cells expressing Ankrd11 (H), Ki67 (J) or βIII-tubulin (K). *$p<0.05$, **$p<0.01$, n = 3 experiments. Arrows in (I) denote double-positive cells. (L-R) E13/14 cortices were electroporated with EGFP and control (Con) or *Ankrd11* shRNA (sh2), and sections were immunostained 3 days later for EGFP (green, L,N), Pax6 (red, N) and Ki67 (blue, N) or phospho-histone H3, and quantified for the relative location of EGFP-positive cells (M), or the proportions of EGFP-positive, Pax6-positive cells (O), EGFP-positive, Ki67-positive cells (P), EGFP-positive, Pax6-positive cells that also expressed Ki67 (Q), or EGFP-positive, phospho-histone H3-positive cells (R). In (L) arrows denote cells in the CP, while (N) shows confocal images of the VZ/SVZ, with arrows denoting triple-positive cells and arrowheads EGFP-positive, Pax6-positive, Ki67-negative cells. *$p < 0.05$, **$p < 0.01$, ***$p < 0.005$, n = 3 embryos each. Scale bars, (A,F,I) = 10 μm, (L,N) = 20 μm. Error bars indicate S.E.M. **See also Figure S2.**

Figure 3. ***Ankrd11 knockdown in cortical precursors perturbs the numbers and positions of developing neurons.*** (A-G) E13/14 cortices were electroporated with EGFP and control (Con) or *Ankrd11* shRNA (sh1 or sh2), and sections were immunostained 3 (A-C) or 4 (D-G) days later for EGFP (green) and HuD (red, A), Satb2 (red, D) or Tbr1 (red, E), and quantified for the proportions of EGFP-positive cells expressing HuD (B) or Satb2 and Tbr1 (F) or the relative location of EGFP-positive, marker-positive cells (C,G). In (A,D,E) higher magnification images of double-labelled cells (arrows) are shown at the bottom. *$p < 0.05$, **$p < 0.01$, n = 3 embryos each. (H-N) E13/14 cortices were electroporated with PB transposase and PB EGFP reporter and

control (Con) or *Ankrd11* (sh2) shRNA, and sections were immunostained at P3 for EGFP (green), and Satb2 (red, I) or Tbr1 (red, J), and quantified for the relative location of EGFP-positive, marker-positive cells in the different cortical layers (K,M,N) or the proportions of EGFP-positive cells expressing Satb2 or Tbr1 (L). In (I,J), higher magnification images of double-labelled cells (arrows) are shown at the bottom. *p < 0.05, **p < 0.01, ***p < 0.005, n = 3 each. Scale bars = 20 μm. Error bars indicate S.E.M. **See also Figure S3.**

Figure 4. ***Ankrd11$^{Yod/+}$ embryos display deficits in cortical precursor proliferation, neuronal numbers and neuronal localization.*** (A) Schematic of Ankrd11 showing the Yoda missense mutation (Barbaric et al., 2008), and a human deletion in the same region (Sirmaci et al., 2011). (B-E) E18.5 *Ankrd11$^{Yod/+}$* (Yoda) and wildtype (WT) cortical sections were immunostained for Tbr1 (B) or Satb2 (C), and the relative location of Tbr1-positive (D) and Satb2-positive (E) neurons quantified. Arrows in (B,C) denote misplaced neurons in the VZ/SVZ. *p < 0.05, **p < 0.01, ***p < 0.001, n = 4 each. (F-L) E18.5 cortical sections from *Ankrd11$^{Yod/+}$* (Yoda) and wildtype (WT) embryos BrdU-labelled at E13.5 were immunostained for BrdU (red,G,I,J) and Ki67 (green, I) or Satb2 (green, J), and quantified for relative location of BrdU-positive cells (H), BrdU-positive, Ki67-positive cells in the VZ/SVZ (K) or total BrdU-positive, Satb2-positive cells (L). To define the cortical regions in (G,H) E18.5 sections were immunostained for Pax6 (green, F), Satb2 (red, F) and Tbr2 (see Figure S4C). The IZ/CP border for quantification was defined by the apical-most edge of the Satb2-positive neurons in the wildtype sections, as shown by hatched lines. (I) shows only the VZ/SVZ and dotted lines indicate the apical edge. Arrows denote single (G) or double-labelled (I,J) cells. *p < 0.05, **p < 0.01, n = 4 each. Scale bars = 20 μm. Error bars indicate S.E.M. **See also Figure S4.**

Figure 5. ***Perturbations in neural precursors, adult-born neurons and behavior in adult Ankrd11$^{Yod/+}$ mice.*** (A-J) Adult six month old *Ankrd11$^{Yod/+}$* (Yoda) mice and their wildtype littermates (WT) were injected with BrdU and the SVZ, olfactory bulb (OB), or dentate gyrus (DG) were analyzed 24 hours (A-C, F-I) or 30 days (D,E,J) later. (A-C) Sections spanning the SVZ 24 hours post-injection were immunostained for BrdU (green, A) and Sox2 (red, A), and total BrdU-positive cells (B) and percentage of Sox2-positive cells that were BrdU-positive (C) quantified. Arrows denote double-labelled cells. **p<0.01, ***p<0.001, n = 3 animals each.

(D,E) Sequential olfactory bulb sections 30 days post-injection were immunostained for BrdU (green, D) and NeuN (red, D), and total BrdU-labelled, NeuN-positive neurons quantified (E). Arrows show double-labelled neurons. *p<0.05, n = 3 each. (F-I) Quantification of sections 24 hours post-BrdU injection for total subgranular zone (SGZ) cells that were BrdU-positive (F), Sox2-positive (G), BrdU- and Sox2-positive (H) or doublecortin-positive (I). ***p < 0.001, n = 3 each. (J) Quantification 30 days post-injection for total BrdU-positive, NeuN-positive dentate gyrus neurons. ***p < 0.001, n = 3 each. (K-O) Adult *Ankrd11*$^{Yod/+}$ (Yoda) and wildtype (WT) littermates were analyzed behaviorally. (K) Total distance travelled (cm) in the open field test. *p < 0.05, n = 15 WT and 9 *Ankrd11*$^{Yod/+}$ mice. (L,M) Percentage of time spent (L) in the stranger 1 (Str1) chamber versus the empty container (Emt) chamber and (M) in the stranger 1 (Str1) chamber versus the new stranger 2 (Str2) chamber during the three chamber sociability test. *p<0.05, **p < 0.01, two way repeated measures ANOVA (genotype X side) with Bonferroni 's post hoc analysis, n = 15 WT and 9 *Ankrd11*$^{Yod/+}$ mice, ns = not significant. (N) Social novelty index, calculated as [$time_{Str2}$/($time_{Str2}$ + $time_{Str1}$)]x100-50 (Jamain et al., 2008). *p<0.05, n = 15 WT and 9 *Ankrd11*$^{Yod/+}$ mice. (O) Total time spent self-grooming (seconds) over a 10 minute test period. **p<0.01, n = 15 WT and 7 *Ankrd11*$^{Yod/+}$ mice. Scale bars, (A,D) = 100 μm. Error bars indicate S.E.M. **See also Figure S5.**

Figure 6. ***Alterations in self-renewal and gene expression in embryonic cortical precursors from Ankrd11*$^{Yod/+}$ *mice.*** Analysis of *Ankrd11*$^{Yod/+}$ (Yoda) and wildtype (WT) E14 cortical neurospheres. (A,B) Number of (A) primary and (B) secondary neurospheres generated from E14 cortical cells at clonal density **p < 0.01, ***p<0.005, n = 6 WT and 7 *Ankrd11*$^{Yod/+}$ embryos. (C-E) Microarray analysis of 6 and 5 independent isolates of *Ankrd11*$^{Yod/+}$ and wildtype secondary cortical neurospheres (Yoda1-6 and WT1-5). (C) Spearman rank correlation matrix computed for the microarray experiments based upon all 41345 probe sets, with red and blue representing the most and least highly correlated samples, respectively. (D) Venn diagram of a pair-wise comparison showing genes that were significantly different (using FDR p-value < 0.1 and FC > 1.1 or < -1.1). (E) A heatmap of the 761 genes that were significantly differentially expressed in (D), clustered using Partek Genomics Suite. The genes are shown in Table S1. (F) qRT-PCR analysis of genes selected from the microarray analysis. *p<0.05, **p<0.01, n = mRNA from 6 secondary neurosphere samples each. (G) Correlation of fold-change in gene

expression (*Ankrd11*$^{Yod/+}$ versus WT neurospheres) for the microarrays versus the qRT-PCRs. Each point represents the average value of genes in (F) from at least 6 mRNA preparations each. Pearson's correlation coefficient R^2=0.995, p=0.00003. (H) Significantly differentially expressed genes from (E) were analyzed using Ingenuity pathway analysis, and the top pathways are presented. Categories are color-coded based on the number of genes they contain. Genes in each category are shown in Table S2. **See also Tables S1 and S2.**

Figure 7. ***Ankrd11 associates with chromatin, histone acetylation is increased in Ankrd11***$^{Yod/+}$ ***neural precursors, and this causes decreased precursor proliferation.*** (A-C) Western blots with acetylation-site specific histone antibodies (H4K5ac, H4K8ac, H3K9ac, H4K16ac, H3K14ac, H3K27ac) in (A) total histones isolated from adult *Ankrd11*$^{Yod/+}$ (Yoda) and wildtype (WT) cortices or (B) in chromatin protein from E14 cortical secondary neurospheres. Samples were also probed for total histone H4, and (C) shows chemiluminescence quantification relative to H4 of blots as in (B). *p < 0.05, n = 7 neurosphere samples each. (D) ChIP-qPCR of E14 cortical neurosphere chromatin immunoprecipitated with anti-H4K16ac or anti-H4. Genomic loci associated with anti-H4K16ac or anti-H4 were expressed as percent input, and H4K16ac values were normalized to total H4 values. *p<0.05, **p<0.01, n = 5 neurosphere samples each. (E) ChIP-qPCR of wildtype E14 neurosphere chromatin immunoprecipitated with anti-Ankrd11 or non-specific IgG (dashed line). Genomic loci associated with anti-Ankrd11 or IgG were expressed as percent input and normalized to IgG (equated to 1). Blue and grey bars designate loci that were significantly (*p<0.05, **p<0.01) or not significantly associated (n.s.) with Ankrd11, respectively. n = 4 E14 cortical neurosphere samples. (F) Confocal images of E12.5 cultured cortical precursor nuclei immunostained for Ankrd11 (green) and HDAC3 (red). The boxed areas are also shown at higher magnification on the bottom. Arrows denote colocalization. (G) Cortical precursor nuclei (blue, Hoechst) following the proximity ligation assay with anti-HDAC3 and anti-Ankrd11 (right, red puncta) or, as a negative control, anti-eIF4E and anti-Ankrd11 (left). (H,I) E12.5 precursors were cotransfected with EGFP and control (Con) or *Ankrd11* (sh2) shRNA. In (H) cells were treated with 500 nM C646 HAT inhibitor after 2 days and in (I) they were also cotransfected with a control or HDAC3 expression vector. Three days post-transfection cells were immunostained for EGFP and Ki67 and quantified. **p<0.01, ***p < 0.001, analyzed by ANOVA with Fisher's posthoc test. n = 3 experiments each. Scale bars, (F)

= 5 μm, (G) = 10 μm. Error bars indicate S.E.M. **See also Figure S6.**

Figure 1
Click here to download high resolution image

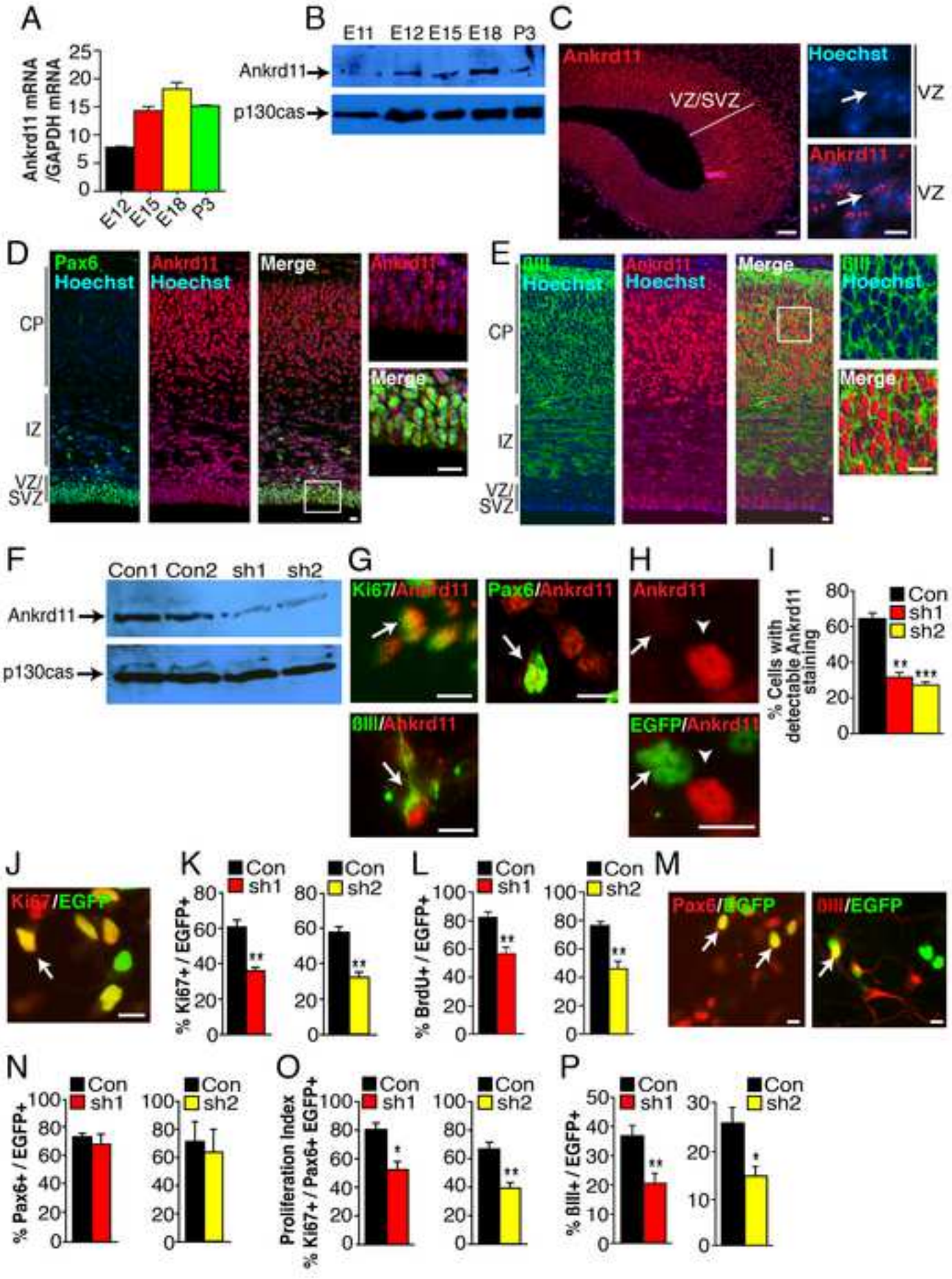

Figure 2

Click here to download high resolution image

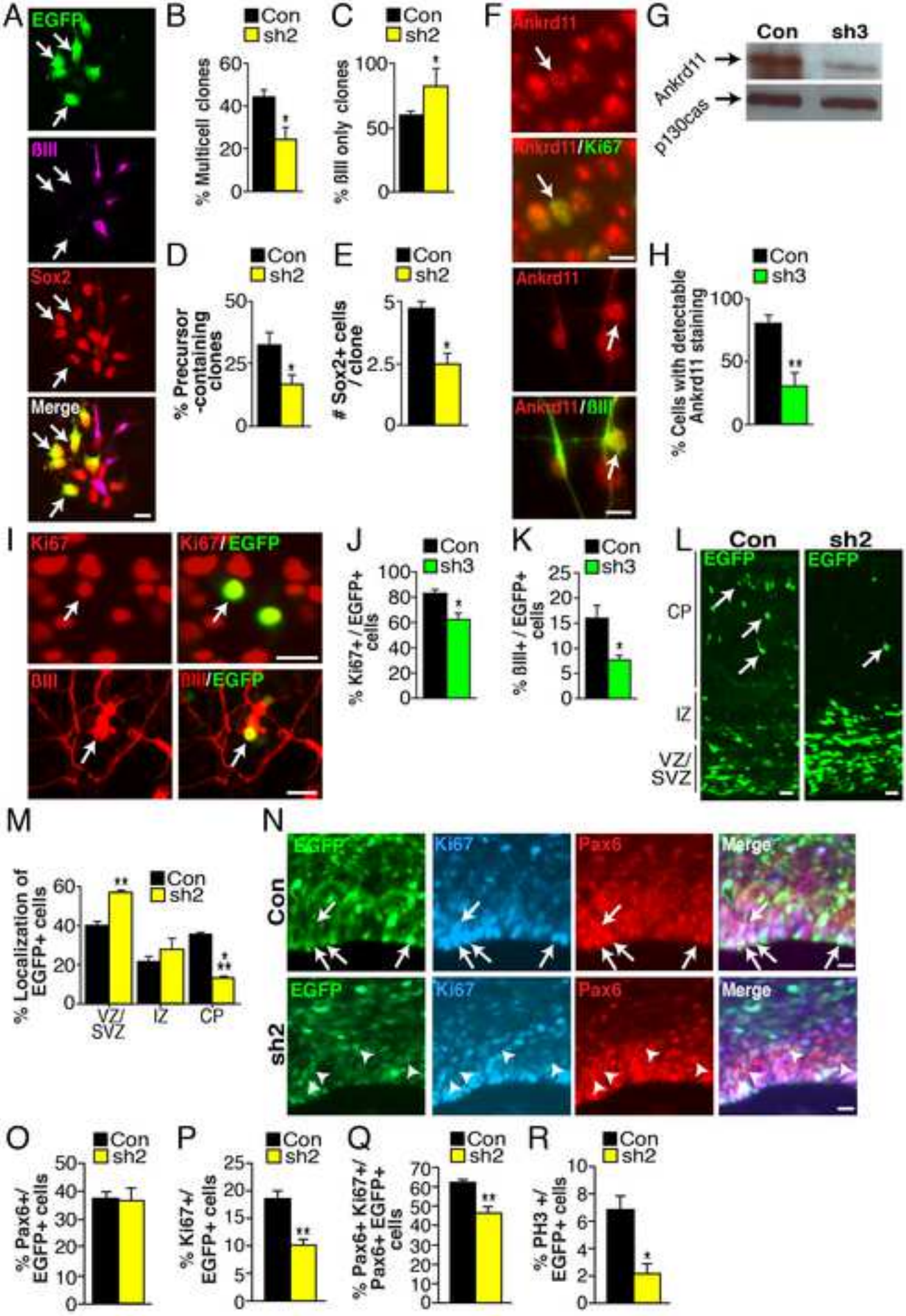

Figure 3

Click here to download high resolution image

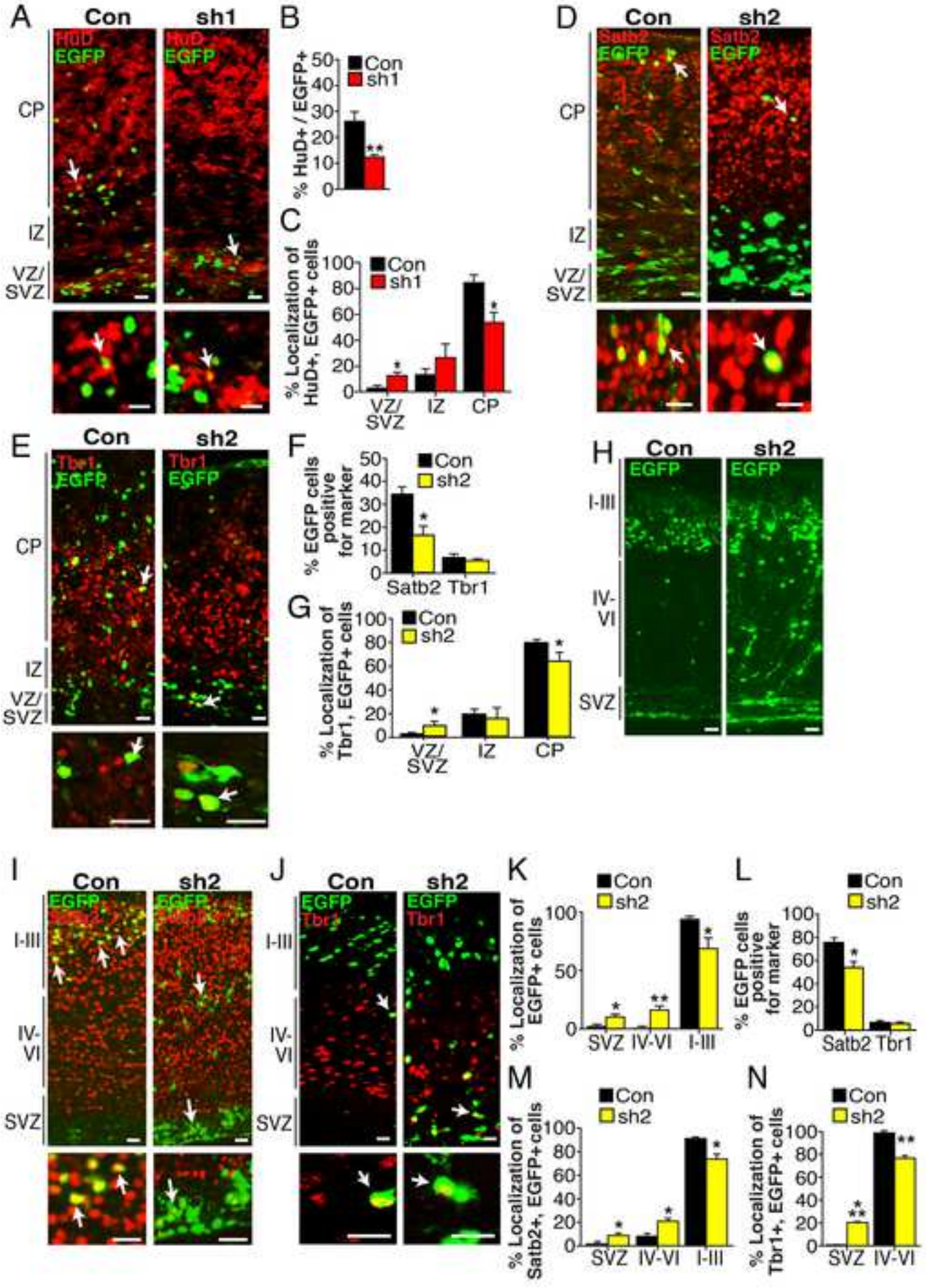

Figure 4

Click here to download high resolution image

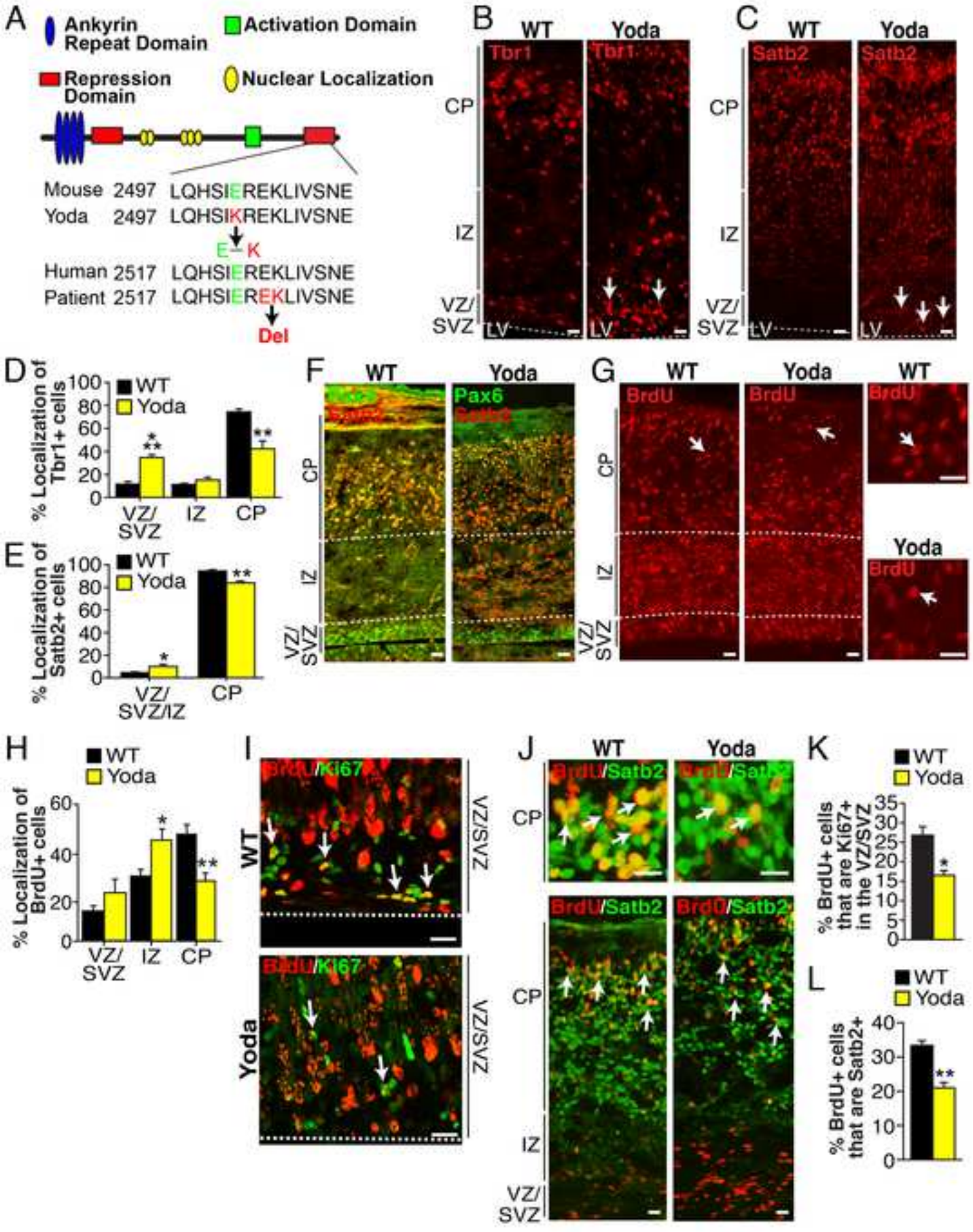

Figure 5
Click here to download high resolution image

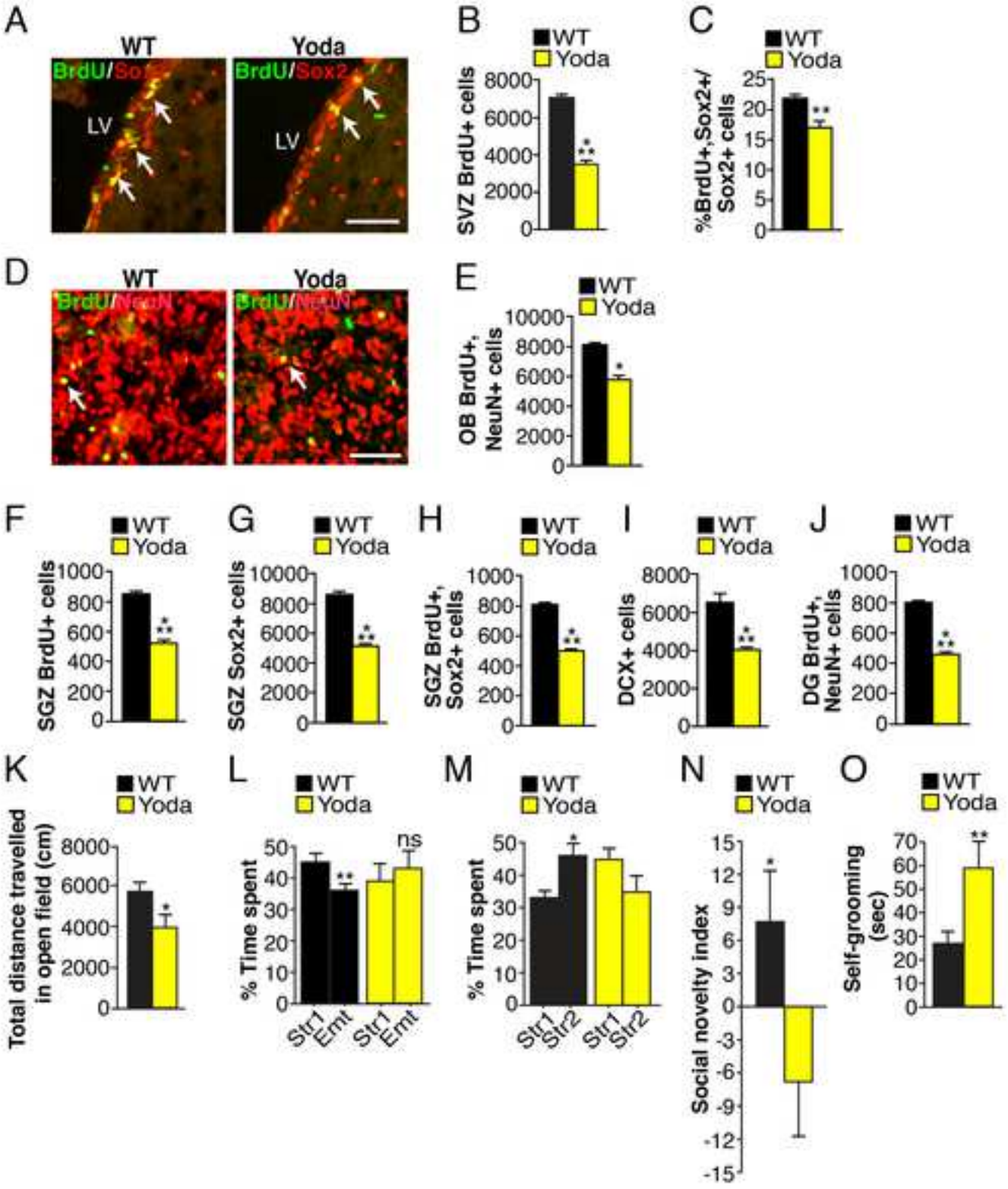

Figure 6

Click here to download high resolution image

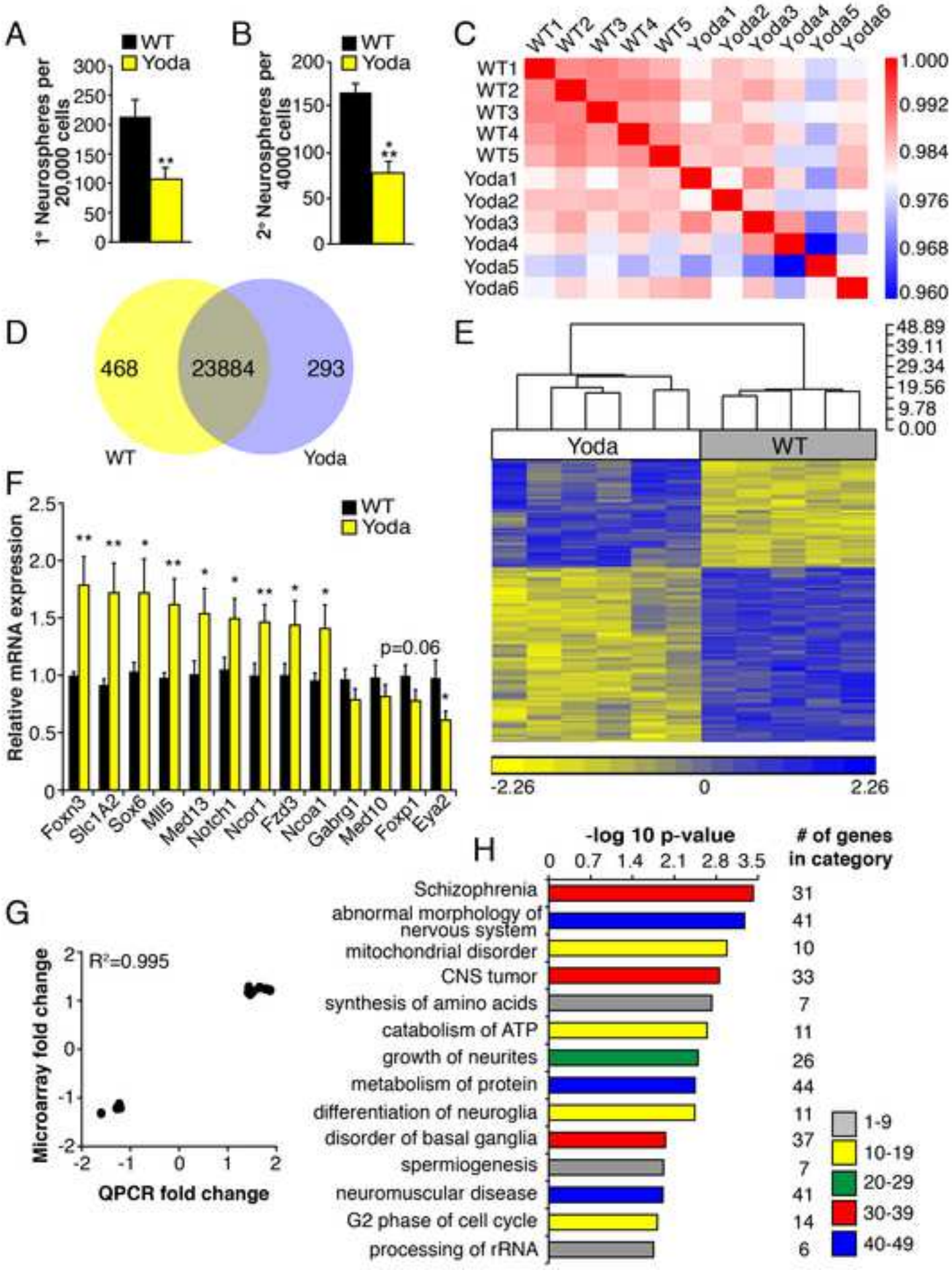

Figure 7
Click here to download high resolution image

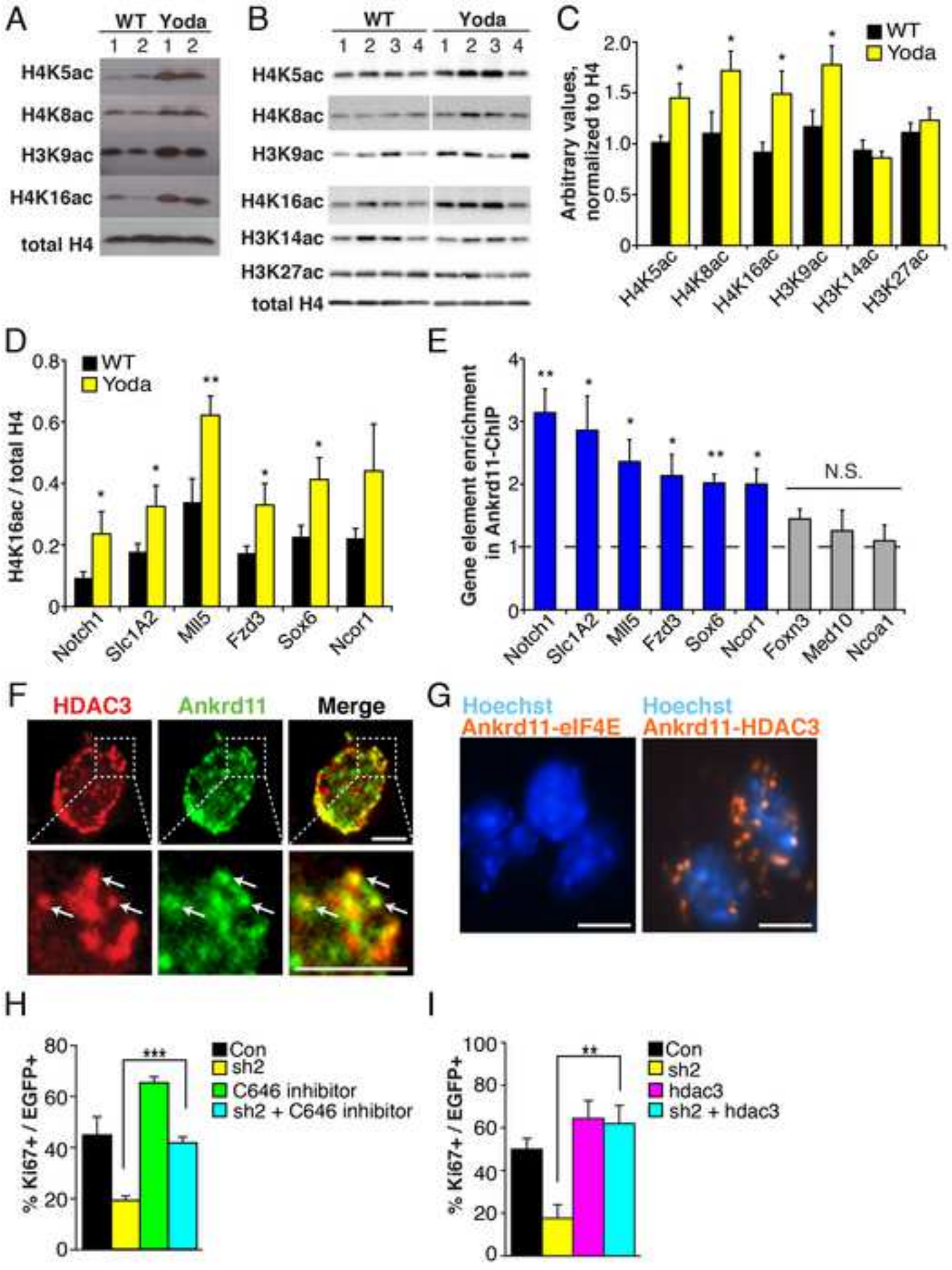

SUPPLEMENTAL MATERIALS

Supplemental Figures and Figure Legends

Figure S1, related to Figure 1.

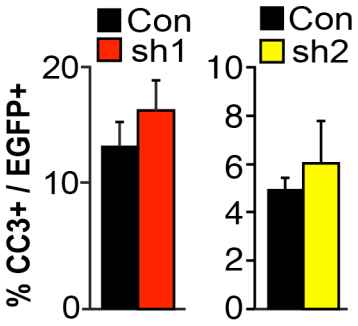

Figure S1. ***Ankrd11 knockdown does not affect cell survival.*** E12.5 murine cortical precursors were cotransfected with a nuclear EGFP plasmid, and a control shRNA (Con) or one of two *Ankrd11* shRNAs (sh1 or sh2), and analyzed by immunostaining 2 days later. Graphs indicate the proportion of EGFP-positive precursors that expressed cleaved caspase-3 (CC3). $p > 0.05$, $n = 3$ independent experiments.

Figure S2, related to Figure 2.

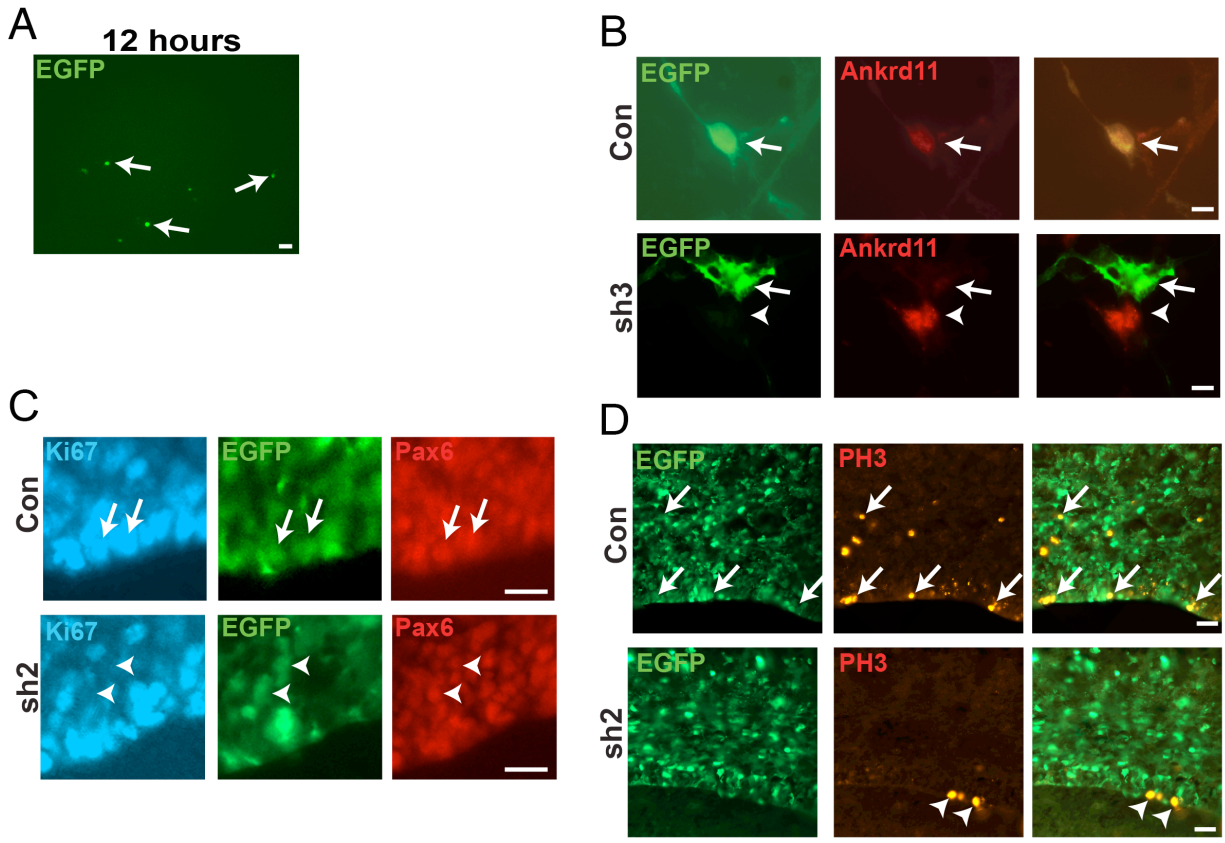

Figure S2. ***Analysis of the effects of Ankrd11 knockdown on cortical precursor self-renewal in culture and in vivo.*** (A) Images of E12.5 cultured cortical precursors that were cotransfected with the PB transposase plasmid, the PB EGFP reporter plasmid, and control shRNA, and analyzed 12 hours later, showing the sparse EGFP-positive cells (arrows) which comprise, at most, 1-3% of total cells in the cultures. (B) Images of human cortical precursor cultures 3 days following transfection with a nuclear EGFP plasmid and control or Ankrd11 shRNA (sh3), immunostained for EGFP (green) and Ankrd11 (red). Arrows in the top panels denote a control shRNA-transfected cell expressing detectable Ankrd11. Arrows in the bottom panels denote an EGFP-positive Ankrd11 shRNA-transfected cell that is negative for Ankrd11 beside a nontransfected cell that is Ankrd11-positive (arrowhead). (C,D) E13/14 murine cortices were electroporated with a nuclear EGFP plasmid and control (Con) or *Ankrd11* shRNA (sh2), and coronal cortical sections were immunostained 3 days later. (C) High magnification images of the VZ/SVZ immunostained for EGFP (green), Pax6 (red) and Ki67 (blue). Arrows denote triple-positive cells and arrowheads EGFP-positive, Pax6-positive cells that are negative for Ki67. (D)

Images of the VZ/SVZ immunostained for EGFP (green) and phospho-histone H3 (PH3, red). Arrows denote double-labelled cells. Scale bars, (A) = 100 μm, (B) = 10 μm, (C,D) = 30 μm.

Figure S3, related to Figure 3.

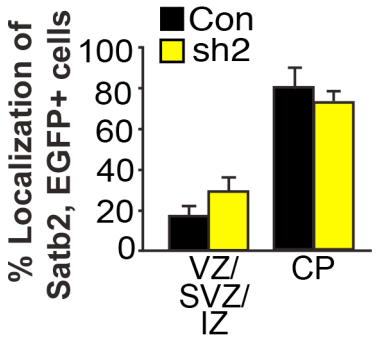

Figure S3. ***Analysis of newborn cortical neurons following Ankrd11 knockdown in vivo*****.** E13/14 cortices were electroporated with a nuclear EGFP plasmid and control (Con) or *Ankrd11* (sh2) shRNA, and coronal cortical sections were immunostained 4 days later for EGFP and Satb2. The graph shows the proportion of double-labelled cells found in the different cortical regions. $p>0.05$, n = 3 embryos each. Error bars indicate S.E.M.

Figure S4, related to Figure 4.

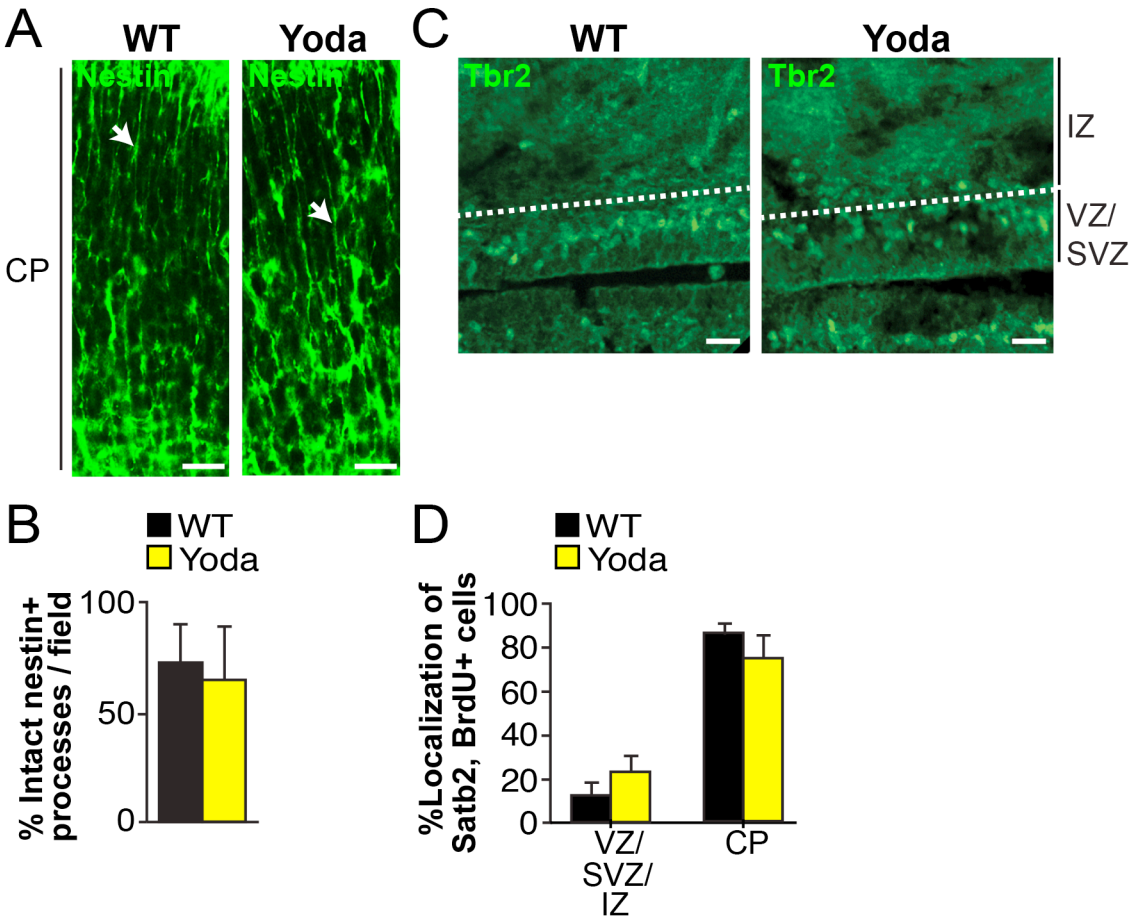

Figure S4. ***Analysis of radial precursor processes in Ankrd11$^{Yod/+}$ embryos.*** (A,B) Coronal cortical sections from E18.5 *Ankrd11$^{Yod/+}$* mice (Yoda) and their wildtype (WT) littermates were immunostained for nestin (green, A), and the relative proportion of basally-oriented nestin-positive processes in the CP was quantified (B). $p>0.05$, n = 3 embryos each. (C) Cortical sections from E18.5 wildtype and *Ankrd11$^{Yod/+}$* embryos were triple-labelled for Pax6, Satb2 (both shown in Figure 4F) and Tbr2 (green, above). (D) Wildtype mothers were crossed to *Ankrd11$^{Yod/+}$* males, injected with BrdU on E13.5, and coronal cortical sections from their *Ankrd11$^{Yod/+}$* (Yoda) and wildtype progeny were immunostained on E18.5 for BrdU and Satb2. The graph shows the proportion of double-labelled cells found in the different cortical regions. $p>0.05$, n = 4 each. Scale bars, (A) = 40 μm, (C) = 20 μm. Error bars indicate S.E.M.

Figure S5, related to Figure 5.

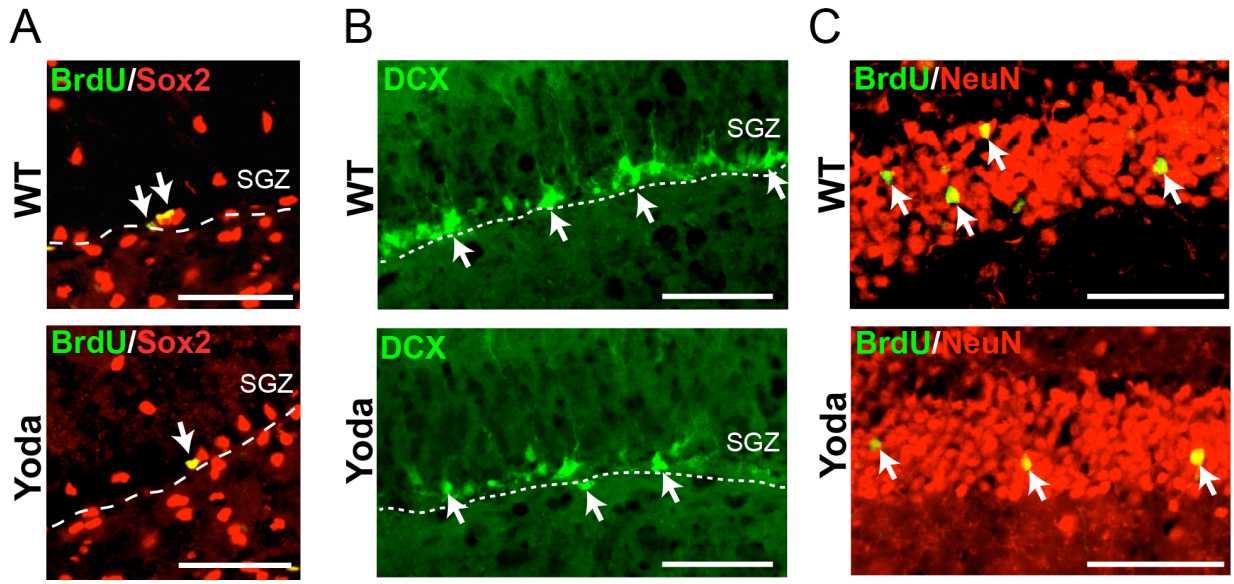

Figure S5. ***Analysis of NPCs and adult-born neurons in the dentate gyrus of adult Ankrd11$^{Yod/+}$ mice.*** Adult six month old *Ankrd11$^{Yod/+}$* (Yoda) mice and their wildtype littermates (WT) were injected with BrdU and the dentate gyrus was immunostained 24 hours (A,B) or 30 days (C) later for BrdU (green, A and C), and Sox2 (red, A) or NeuN (red, C), or for doublecortin (green, B). Arrows denote double-positive (A,C) or single-positive (B) cells. Hatched white lines denote the boundary of the SGZ. Scale bars, (A-C) = 100 μm.

Figure S6, related to Figure 7.

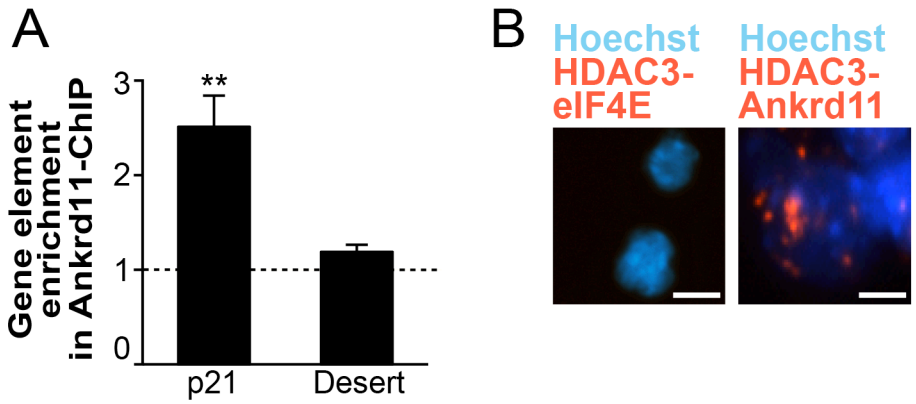

Figure S6. ***Ankrd11 associates with chromatin and with HDAC3.*** (A) ChIP-qPCR analysis of chromatin from wildtype E14 neurospheres immunoprecipitated with anti-Ankrd11 or non-specific IgG (dashed line). p21 or desert genomic loci associated with Ankrd11 or IgG were expressed as percent input and normalized to IgG (equated to 1). n = 4, **p<0.01. (B) Images of cortical precursor nuclei (blue, Hoechst) following the proximity ligation assay with antibodies for HDAC3 and Ankrd11 (right panel, red puncta) or, as a negative control, eIF4E and HDAC3 (left panel). Scale bars, (B) left panel = 10 μm, right panel = 5 μm. Error bars indicate S.E.M.

Supplemental Excel Table Legends

Supplemental Table S1, related to Figure 6. ***Table containing differentially expressed genes in wildtype (WT) and Ankrd11$^{Yod/+}$ (Yoda) secondary neurospheres.*** This table can be found in a separate Excel file and contains a list of differentially expressed genes in wildtype (WT) and Ankrd11$^{Yod/+}$ (Yoda) secondary neurospheres with false discovery (FDR) p-value < 0.1 and fold change (FC) > 1.1 or < -1.1.

Supplemental Table S2, related to Figure 6. ***Table containing differentially expressed genes from Table S1 that were enriched in pathways depicted in Fig. 6H.*** This table can be found in a separate Excel file and contains a list of differentially expressed genes from Table S1 that were enriched in pathways depicted in Fig. 6H.

Supplemental Experimental Procedures

Yoda mouse genotyping. Endpoint genotyping was performed to detect the Yoda mutation using the AB7500FAST machine. The Yoda allele was detected by 6FAM-labelled probe 1 and the wild type allele detected by VIC-labelled probe 2 below. The forward primer used was 5'-AGCTTAAGATCCTTGCCAGCAT-3' and the reverse primer was 5'-AGGAGCTGTTCAAGCAACAAGAG-3'. The sequences of the labeled probes were as follows; Probe 1 5'-ACTTACCCTCTTGATGCT-3' and Probe 2, 5'-CCCTCTCGATGCTG-3'.

shRNA target sequences. The sequence targeted by murine shRNA1 was 5'-GGACGTGAGTGTTTCCATA 3', by murine shRNA2 was 5'-GGAAGCAGGAACACCGAAA-3', by human shRNA3 was 5'-CCGTATTGAAATGGAGTCAAA-3'and the control shRNA was 5'-GTTCTCCGAACGTGTCACGT-3'.

Human embryonic stem cell differentiation. Briefly, neuralized embryoid bodies were harvested, washed and treated for 12 days with SMAD inhibitors dorsomorphin (2 μM) and SB43152 (10 μM). Embryoid bodies were then dissociated and plated for a further 10 days and Pax6 positive neural precursors were transfected as described below.

Transfection protocol. For transfections, we mixed 1 μg DNA, 1.5 μl of Fugene 6 (Roche) and 100 μl Opti-MEM, incubated for 60 min, and added to cortical precursors 1 hour after plating. Transfections of human neural precursors were performed with 1 μg DNA total, at a 1:2 ratio of EGFP to shRNA or overexpression plasmids, or a 1:1 ratio of PB plasmid and PB EGFP plasmids for clonal analysis. Transfection efficiency ranged from 1-3% of plated cells.

In utero electroporation and in vivo analyses. The square electroporator CUY21 EDIT (TR Tech, Japan) was used to deliver five 50 ms pulses of 40V with 950 ms intervals per embryo. Cells were labelled as indicated by injecting a 1:3 ratio of pEF-EGFP to shRNA plasmid or a 1:1:3 ratio of PCAG-PB-GFP, pCyL43-Pbase , and shRNA or control plasmids for 4 μg total. Brains were dissected in ice-cold HBSS, fixed in 4% paraformaldehyde at 4ºC overnight, cryoprotected and cryosectioned coronally at 16-20 μm. Cell location was measured using NorthernEclipse software (Empix) using a Sony XC-75CE CCD video camera and delineating

the VZ/SVZ, IZ and CP using Hoechst staining or by immunostaining of markers. For all experiments at least 3 embryos from at least 2 different mothers were analyzed.

BrdU analyses. Specifically, for embryonic analyses pregnant mice were injected with BrdU (Sigma) dissolved in PBS at a dose of 100 mg per kg of body weight at gestational day 13.5 and the cortices of their embryonic progeny were analyzed 5 days later. For immunostaining of sections from these embryos, sections were dried for 20 minutes, incubated in 0.5 N HCL for 30 minutes at 60°C and washed in 1X PBS buffer for 5 minutes before blocking and immunostaining as described here and in the main methods.

qRT-PCR and Microarray. RNA was isolated using Trizol and the RNeasy Mini kit (Qiagen), and reverse-transcribed with the Omniscript Reverse Transcription Kit and random hexamers (Qiagen). RNA for microarrays was isolated from secondary neurospheres 5 days post-passage using E.Z.N.A. total RNA or MicroElute Total RNA kit (Omega Biotek) and cDNA prepared using 250 ng of total RNA and Ambion Whole Transcriptome (WT) kit (Applied Biosystems). Primer sequences were designed using Primer3 software (Untergrasser et al., 2012) or used from the PrimerBank (Spandidos et al., 2010). All primers were validated and qPCR assays were performed in accordance with MIQE guidelines (Bustin et al., 2009). Gene expression was quantified using SYBR Green PCR Master Mix (Applied Biosystems) and the ABI Prism® 7900HT sequence detection system and analyzed with Sequence Detector System 2.2.1 software (both Applied Biosystems). For microarray validation, cDNA was assayed by qPCR using the LightCycler® 480 SYBR Green I Master kit and LightCycler® 480 instrument as per manufacturer's instructions (Roche Applied Sciences). Data were normalized to GAPDH and calculated using the $2^{-\Delta\Delta Ct}$ method (Livak and Schmittgen, 2001). Primer sequences are listed in the supplemental tables below.

Western blots Cortices were dissected and lysed in RIPA buffer (50 mM Tris, pH = 8, 150 mM NaCL, 1% NP40, 0.1% SDS, 1 mM EDTA) containing 1 mM PMSF, 1 mM sodium vanadate, 20 mM sodium fluoride, 10 μg/ml aproteinin and 10 μg/ml leupeptin. 50 μg protein lysate was run on a 10% SDS-PAGE gel, and western blots performed as described (Barnabé-Heider et al., 2005). For western blot analysis of histone acetylation, cortical tissue was lysed in Triton extraction buffer (PBS, Triton X100 v/v, 2 mM phenylmethylsulfonyl fluoride, 0.02% NaN3, 5 mM sodium butyrate) on ice. The lysate was centrifuged at 6500xg for 10 minutes, the nuclear

pellet was washed in extraction buffer and resuspended in 0.2N HCl overnight at 4° C. All samples were centrifuged to pellet debris and a Bradford assay was used to determine the concentration of histone protein in the supernatant. 1.5 μg of total histone protein was run on precast 4-15% Mini PROTEAN TGX gels (Biorad), and protein was transferred onto nitrocellulose. Membranes were blocked in 5% BSA (Fisher Science) in TBS-T, probed with primary antibodies diluted in TBST at 4°C overnight, incubated with secondary antibodies for 30 minutes at room temperature, washed, and incubated in Enhanced Chemiluminescence (GE Healthcare) for detection.

Antibodies for western blots. Primary antibodies were anti-Ankrd11 (Neilsen et al., 2008), anti-p130cas (1:2000; Abcam), anti-H3K9ac (1:2000; Millipore), anti-H3K14ac (1:1000; Millipore), anti-H3K27ac (1:1000; Millipore), anti-H4K5ac (1;2,000; Millipore), anti-H4K8ac (1:2000; Millipore), anti-H4K16ac (1:5,000; Millipore) and anti-total H4 (05-858, 1:20000; Millipore). Secondary antibodies were goat anti-rabbit HRP (1:10,000; Millipore) and goat anti-mouse HRP (1:10,000; GE Healthcare).

ChIP analysis. Secondary neurospheres 5 days post-passage were gently triturated and then cross-linked in 1% formaldehyde (Calbiochem) for 5 minutes at room temperature. The reaction was stopped by adding glycine to a final concentration of 0.125M. Cells were washed with PBS and subjected to chromatin isolation as described in (Savage et al., 2009) except that chromatin was sheared to 200-500 base pairs in size using Covaris S2 in 1 ml AFA tubes for 12 minutes (Covaris Inc.). Sheared chromatin was centrifuged at 14,000 g for 15 minutes at 4°C and soluble chromatin was frozen as single use aliquots. To analyze chromatin associated with Ankrd11, 20 μg of chromatin was immunoprecipitated with 4 μg of anti-Ankrd11 (Neilsen et al., 2008) or non-specific rabbit IgG (Millipore) as described in (Savage et al., 2009). To analyze chromatin associated with H4K16ac, 2 μg of chromatin was immunoprecipitated with 2 μg of antibodies targeted to H4K16ac or total H4 (Millipore) as described above. Eluted chromatin was reverse-crosslinked at 65°C for 16 hours and then treated with 20 μg of RNAse A and 40 μg of proteinase K. DNA was purified using QiaQuick PCR purification kit (Qiagen). Ankrd11-, H4K16ac- and total H4-bound chromatin was calculated as percent input by qPCR assay using the LightCycler® 480 SYBR Green I Master kit and LightCycler® 480 instrument as per manufacturer's instructions (Roche Applied Sciences). All primers were validated and qPCR assays were performed in accordance with MIQE guidelines (Bustin et al., 2009).

Antibodies for immunochemistry and PLA. The primary antibodies were rabbit anti-Ankrd11 (Neilsen et al., 2008), mouse anti-GFP (1:1000, Invitrogen), rabbit anti-GFP (1:400, Chemicon), chicken anti-GFP (1:1000, Abcam), mouse anti-βIII-tubulin (1:1000, Covance), rabbit anti-βIII-tubulin (1:1000, Covance), rat anti-BrdU (1:200, Accurate Chemical), anti-Sox2 (1:100, Santa Cruz), goat anti-doublecortin (1:500, Santa Cruz), anti-NeuN (1:100, Santa Cruz), anti-Pax6 (1:2000, Covance), anti-Ki67 (1:400, BD Biosciences), anti-Tbr1 (1:400, Abcam), anti-Tbr2 (1:500, Millipore), anti-Satb2 (1:500, Abcam), rabbit anti-pH3 (1:250, Millipore), anti-HDAC3 (1:500, Abcam), anti-nestin (1:500, BD Biosciences), mouse anti-eIF4E (1:500, BD Pharmingen), rabbit anti-eIF4E (1:250, Cell Signaling) and rabbit anti-cleaved caspase 3 (1:200, Millipore). The secondary antibodies used for immunocytochemistry were indocarbocyanine- (Cy3) or Alexa555-conjugated goat anti-mouse and anti-rabbit IgG (1:400, Jackson ImmunoResearch or 1:1000, Invitrogen), FITC- or Alexa 488-conjugated anti-mouse and anti-rabbit IgG (1:200, Jackson ImmunoResearch or 1:1000, Invitrogen), dichlorotriazinyl amino fluorescein-conjugated streptavidin (1:1000, Jackson ImmunoResearch), Cy3-conjugated streptavidin (1:1000, Jackson ImmunoResearch), Alexa 488-conjugated chicken anti-rat (1:400, Molecular Probes), and Alexa 555-conjugated goat anti-mouse (1:500, Molecular Probes). For PLA, cells were incubated with rabbit anti-Ankrd11, mouse anti-HDAC3, and/or anti-eIF4E or, for the negative controls, rabbit anti-eIF4E. Cells were treated with Duolink probes, and ligation and amplification solutions as per manufacturer's instructions (Olink Bioscience).

Adult neurogenesis assays. Brains were postfixed overnight, cryopreserved in 20-30% sucrose and the SVZ and SGZ were sectioned coronally on a cryostat at 18 μm. Ten SVZ or dentate gyrus sections, sampled every tenth section, were analyzed immunohistochemically for BrdU as described (Cancino et al., 2013). For the SVZ and dentate gyrus, we quantified all BrdU-labelled nuclei. To perform the Sox2/BrdU analysis, sections were incubated in 1 N HCl at 60°C for 30 min, rinsed in PBS, incubated in rat anti-BrdU antibody at 4°C overnight, and then in Alexa 488 donkey anti-rat antibody for 2 hours followed by sequential immunostaining with anti-Sox2 followed by an Alexa Fluor 555-conjugated donkey anti-mouse secondary antibody. The total numbers of Sox2-positive, BrdU-positive, and double-labelled Sox2/BrdU-positive cells were then quantified in 10 sections through the SVZ or dentate gyrus, sampled every ten serial sections. To quantify adult-born olfactory bulb or hippocampal neurons, adult wildtype and *Ankrd11*$^{Yod/+}$ mice were injected with 60 mg/kg BrdU intraperitoneally every 3 hours for five injections. After thirty days, the hippocampi or olfactory bulbs were cryosectioned serially at 18

μm throughout their rostrocaudal extent. Every tenth serial section was immunostained, for a total of 10 sections per brain. To perform immunostaining, sections were incubated in 1 N HCl at 60°C for 30 min, rinsed in PBS, incubated in rat anti-BrdU antibody at 4°C overnight, and then in Alexa 488 donkey anti-rat antibody for 2 hours followed by sequential immunostaining with anti-NeuN followed by an Alexa Fluor 555-conjugated donkey anti-mouse antibody. The total numbers of BrdU-NeuN double labeled cells in the granule cell layers were counted, and to obtain the total relative number of BrdU-positive adult-born neurons, these numbers were multiplied by ten to account for sampling frequency.

Behavioral analyses. Before each test the mice were placed in the testing room for a habituation period of 30 minutes. For evaluation of locomotor activity, mice were placed in the center of a clear Plexiglass (40X40X30 cm) open-field arena and allowed to explore for 30 minutes. Activity in the open-field was quantified by a computer-operated Digiscan optical animal activity system (Accuscan Electronics) containing 16 photoreceptor beams on each side of the arena, which divides the arena into 256 equally sized squares. Total distance (locomotor activity), movement time (seconds), movement speed (cm/second), vertical activity (rearing measured by photobeam interruptions) and center distance (distance traveled in center of the arena) were recorded. Data were collected in 2 minute intervals over the 30 minute test session.

To evaluate social interaction and social recognition, the social behavior apparatus was a rectangular 3 chambered cage made of clear carbonate (Moy et al., 2004; Molina et al., 2008). Dividing walls had retractable doors allowing access to each section of the cage. The entire test video was recorded. The test consisted of 3 intervals of 10 minutes each. In the first 10 minutes (habituation period), the mouse was placed in the center chamber and allowed to explore the whole cage (doors open) and its' position recorded. After the habituation period was complete the test mouse was enclosed in the center compartment, and an unfamiliar mouse (Stranger 1) was placed into a plastic container with openings that allows for visual and smell recognition but prevents direct contact, in one side of the chambers, and an empty container in the other chamber. The doors were opened and the position of the test mouse was recorded for a further 10 minutes. To measure preference for social novelty at the end of the 10 minutes the mouse was enclosed again in the center chamber and a second unfamiliar mouse (stranger 2) was placed in the empty container. The doors were opened again and the position of the tester mouse was

recorded for an extra 10 minutes. Data were analyzed as a percentage of total time spent in each chamber section during each 10 minute interval. The social novelty index was calculated as per Jamain et al. (2008), as $[time_{Str2}/(time_{Str2} + time_{Str1})]x100-50$.

For the self-grooming assay, the tested mouse was transferred to a new cage without bedding for a habituation period of 10 minutes. Following the habituation, an observer recorded with a stopwatch the amount of time the mouse spent self-grooming for a period of 10 minutes.

SUPPLEMENTAL REFERENCES

Bustin S.A., Benes V., Garson J.A., Hellemans J., Huggett J., Kubista M., Mueller R., Nolan T., Pfaffl M.W., Shipley G.L., Vandesompele J., Wittwer C.T. (2009) The MIQE guidelines: minimum information for publication of quantitative real-time PCR experiments. Clin Chem 55:611-622).

Livak, K.J., and Schmittgen, T.D. (2001) Analysis of relative gene expression data using real-time quantitative PCR and the 2(-Delta Delta C(T)) method. Methods *25*, 402-408.

Spandidos A., Wang X., Wang H., and Seed B. (2012): PrimerBank: a resource of human and mouse PCR primer pairs for gene expression detection and quantification. Nucl. Acids Res. 38:D792-9).

Untergrasser A., Cutcutache I., Koressaar T., Ye J., Faircloth B.C., Remm M., Rozen S.G. (2012) Primer3 - new capabilities and interfaces. Nucleic Acids Research 40(15) e(115).

Primer sequences for ChIP-qPCR experiments. F indicates forward primers and R reverse primers.

Primer	Sequence
Desert - F	TCCTCCCCATCTGTGTCATC
Desert - R	GGATCCATCACCATCAATAACC
Foxn3 - F	TGGGAGCACACATACCTTCA
Foxn3 - R	GGCGCGTATTGATTTGTTTT
Frzd3 - F	TCCTCTCCACCGAGACCTTA
Frzd3 - R	GAGCCCTCTAAGCGGAAGAT
Med10 - F	CACATGCCTTTGCTGTGTTT
Med10 - R	AAGCCTTTGAAGGGAAAACC
Mll5 - F	CAGAGGGGGCATAGACACTC
Mll5 - R	TCAGTGGGAACCCAAGAGTC
Ncoa1 - F	AGCTGTGCTTGAGGGAACAG
Ncoa1 - R	GATTCACCTCGTCCTGTCGT
Ncor1 - F	CGTGGCTCCTTAATCTCTGC
Ncor1 - R	GCGGCTAAGAGGAAATGTCA
Notch1 - F	AACCAACAACACGGGTCAAT
Notch1 - R	GCATTCGTTCTGGGACACTT
p21 - F	TCCACAGCGATATCCAGACA
p21 - R	TCCACTCATCACCACACACA
Slc1A2 - F	CCGGTCACCTGAGTGTTTCT
Slc1A2 - R	CCATCACTCCCTGGACATCT
Sox6 - F	TATTCACCGAACCCACCTTC
Sox6 - R	AGTCACATGTCCGGGTTTTC

Primer sequences for RT-qPCR experiments. F indicates forward primers, and R reverse primers.

Primer	Sequence	PrimerBank ID
Eya2 F	ACCGCTGGGCTCTATCAAG	33859550a1
Eya2 R	GGTAGGACGGATAATCCTGGTG	
Foxn3 F	TGCCCGACATCCGATTAGAAG	12856539a1
Foxn3 R	CTAAGGACCGACTCCCCAAAG	
Foxp1 F	AAGTGTTTTGTGCGAGTAGAGAA	16716509a1
Foxp1 R	GGGAAGGGTTACCACTGATCTT	
Fzd3 F	ATGGCTGTGAGCTGGATTGTC	10946846a1
Fzd3 R	GGCACATCCTCAAGGTTATAGGT	
Gabrg1 F	AATCGGATGCACACTGGATAAC	141801939c3
Gabrg1 R	ATGAAGTTGAAGGTAGCACTCTG	
GAPDH F	GGGTGTGAACCACGAGAAATA	N/A
GAPDH R	CTGTGGTCATGAGCCCTTC	
Med10 F	CGTGGAGAACATTCGGCAG	142374083c1
Med10 R	TCTATGTCCTGTAAGCCCGTAAC	
Med13 F	CGACTTGACAGGAATTAAGTGGA	124286861c1
Med13 R	GTCACCGGAAACAGAATAGGG	
Mll5 F	ATGAGCATAGCGATCCCATTG	27370574a1
Mll5 R	TTTCTCAACTACCACAGGGCT	
Ncoa1 F	CGACAACAGTGCTAACGAAGG	6754800a1
Ncoa1 R	CTGCCCTCCTGTAAAAGCC	
Ncor1 F	GCAGTTCCAACCACAAAACCA	26006245a1
Ncor1 R	GGTCTACGTCCATCGGCTC	
Notch1 F	CCGTGTAAGAATGCTGGAACG	31339069a1
Notch1 R	AGCGACAGATGTATGAAGACTCA	
Slc1A2 F	GCCAACAATATGCCCAAGCAG	227330634c1
Slc1A2 R	GACACCAAACACAGTCAGTGA	
Sox6 F	CTGCCTCTGCACCCCATAATG	26326701a1
Sox6 R	TTGCTGAGATGACAGAACGCT	

Supplemental Movies & Spreadsheets

Click here to download Supplemental Movies & Spreadsheets: Supplemental table1.xls

Supplemental Movies & Spreadsheets

Click here to download Supplemental Movies & Spreadsheets: Supplemental table2.xls